





Seasonal dynamics and diversity of Antarctic marine viruses reveal a novel viral seascape

Received: 5 January 2024

Accepted: 4 October 2024

Published online: 24 October 2024

 Check for updates

Gonçalo J. Piedade^{1,2}  , Max E. Schön³ , Cédric Lood^{4,5}, Mikhail V. Fofanov^{4,6}, Ella M. Wesdorp¹, Tristan E. G. Biggs¹ , Lingyi Wu⁶ , Henk Bolhuis¹, Matthias G. Fischer³, Natalya Yutin⁷ , Bas E. Dutilh^{4,6} & Corina P. D. Brussaard^{1,2}  


The Southern Ocean microbial ecosystem, with its pronounced seasonal shifts, is vulnerable to the impacts of climate change. Since viruses are key modulators of microbial abundance, diversity, and evolution, we need a better understanding of the effects of seasonality on the viruses in this region. Our comprehensive exploration of DNA viral diversity in the Southern Ocean reveals a unique and largely uncharted viral landscape, of which 75% was previously unidentified in other oceanic areas. We uncover novel viral taxa at high taxonomic ranks, expanding our understanding of crassphage, polinton-like virus, and virophage diversity. *Nucleocytoviricota* viruses represent an abundant and diverse group of Antarctic viruses, highlighting their potential as important regulators of phytoplankton population dynamics. Our temporal analysis reveals complex seasonal patterns in marine viral communities (bacteriophages, eukaryotic viruses) which underscores the apparent interactions with their microbial hosts, whilst deepening our understanding of their roles in the world's most sensitive and rapidly changing ecosystem.

Viruses are prevalent and numerically dominant agents of microbial mortality, as well as drivers of biodiversity^{1–3}. They play important roles in shaping microbial communities and biogeochemical cycles in the oceans, where two-thirds of living biomass is microbial⁴. Understanding the ecological significance of viruses requires a comprehensive insight into their diversity. Viral metagenomics has revolutionized marine viral ecology^{5–7}, revealing viral community structure, biogeochemical roles, evolutionary trajectories, and taxonomic diversity^{8–13}. Still, key oceanic regions, such as the Southern Ocean, remain understudied¹⁴.

The Southern Ocean, pivotal in global ocean circulation¹⁵, absorbs over 40% of anthropogenic carbon dioxide emissions and hence, plays

a crucial role in moderating climate change¹⁶. This process is significantly driven by microbial activity¹⁷, emphasizing the need for studying the impact of viruses on these microbial hosts. The short polar productive season results in pronounced temporal dynamics in (micro) biological activity and community composition^{18–21}. Substantial seasonal variation was also reported for viral lysis of Antarctic marine microorganisms^{22–26}. Yet, our understanding of the diversity and dynamics of the virus communities remains limited. The few studies that addressed their metagenomic characterization provide a restricted view due to a limited sample number and narrow sampling period^{23,27–30}.

The present study delves into the intricate seasonal variations in Antarctic marine dsDNA virus diversity. It has high temporal resolution

¹Department of Marine Microbiology and Biogeochemistry, NIOZ Royal Netherlands Institute for Sea Research, P.O. Box 59, 1790 AB Den Burg, Texel, The Netherlands. ²Department of Freshwater and Marine Ecology, Institute for Biodiversity and Ecosystem Dynamics (IBED), University of Amsterdam, PO Box 94240, 1090 GE Amsterdam, The Netherlands. ³Max Planck Institute for Medical Research, Department of Biomolecular Mechanisms, 69120 Heidelberg, Germany. ⁴Institute of Biodiversity, Faculty of Biological Sciences, Cluster of Excellence Balance of the Microverse, Friedrich-Schiller-University Jena, 07743 Jena, Germany. ⁵Department of Biology, University of Oxford, 11a Mansfield Road, Oxford OX1 3SZ, UK. ⁶Theoretical Biology and Bioinformatics, Science4Life, Utrecht University, Padualaan 8, 3584 CH Utrecht, the Netherlands. ⁷National Center for Biotechnology Information, National Library of Medicine, National Institutes of Health, Bethesda, MD 20894, USA.  e-mail: goncalo.piedade@nioz.nl; corina.brussaard@nioz.nl

(24 sampling days) over the full productive season in Marguerite Bay, located in the Western Antarctic Peninsula. We advance and expand the catalog of marine viral diversity by combining multiple virus detection and classification approaches tailored to specific viral taxa. Moreover, an improved understanding of seasonal variations in virus-host dynamics highlights the ecological importance of viruses in the Southern Ocean as drivers of diversity and succession. Therefore, this study establishes an essential foundation for understanding the dynamics of this region, which is particularly sensitive to global climate change.

Results

Antarctic viral communities harbor a diverse range of taxa

To explore the dynamics of Antarctic marine viruses and interactions with their hosts, we generated paired metagenomes from viral (< 0.22 μm and free-DNA digestion) and cellular (> 0.22 μm) size fractions. Viral metagenomes, totaling 887 million reads, were co-assembled into 161,651 viral scaffolds, of which 8045 were mid- to high-quality (>10 kb or >70% CheckV³¹ completeness, Supplementary data 1). The viral reads represented 59% of the viral fraction metagenomes, and on average 4% of the reads did not map to the co-assembly (Supplementary Fig. 1a). The sample rarefaction and the species accumulation curves show that we have sequenced deeply enough and with enough sample coverage of the site (Supplementary Fig. 2a, b). The viral fraction metagenomes displayed clear enrichment in viral sequences and depletion in cellular markers (Supplementary Fig. 1a, b). The mid- to high-quality viral sequences clustered into 7957 vOTUs. When comparing the mid- to high-quality viral scaffolds to the Global and Southern Ocean Viromes^{8,29} (GOV and SOV), we found 75% of viral sequences to be novel at the species rank.

The most frequent and abundant viruses were the tailed dsDNA bacteriophages of the class *Caudoviricetes* (Fig. 1a–c), outnumbering other viruses by 53-fold and making up 75% of all scaffolds (Fig. 1b, c). We further categorized *Caudoviricetes* sequences to family rank using PhaGCN²², except the order *Crassvirales* which was characterized using a targeted approach. Seasonal patterns in compositional viral abundance could be discerned for various *Caudoviricetes* taxa, even more pronounced in the cellular fraction (Fig. 1c, d). Differing abundance patterns in the viral and cellular fraction can be the result of seasonal dynamics in lytic and lysogenic viral infection, as the viral reads from the cellular fraction can reflect both actively replicating and lysogenic viral infection while the virus fraction is composed of free viral particles. For example, kyanoviruses displayed different occurrence patterns in the viral and cellular metagenomes, with less reads in the virus fraction than in the cellular metagenome. Similarly, the *Autographiviridae* family sequences were the most abundant (on average 11% viral fraction and 3.5% cellular fraction reads), and displayed increased virus productivity in summer, reflected by the higher abundance in the cellular fraction from mid-January to February (Fig. 1c, d). Few viruses (0.36% reads or 279 scaffolds) were identified as archaeal viruses, which showed higher abundance from November to January (Fig. 1e) and were many classified as *Thumleimavirales* (51 scaffolds).

Abundant eukaryotic viruses belonged to the phylum *Nucleocytoviricota* (originally nucleocytoplasmic large DNA viruses), the classes *Polintoviricetes* (polinton-like viruses or PLVs) and *Maveriviricetes* (virophages), and the family *Circoviridae* (ssDNA; Fig. 1b, c, f). The *Nucleocytoviricota* viruses (NCVs) are the most abundant eukaryotic viruses, accounting for 12.4% and 1.6% of the cellular and viral fraction reads, respectively. NCV abundance in the cellular fraction spiked in March and December 2018, accounting for up to 27% and 77% of viral reads (respectively), implying heightened NCV production.

PLVs form an important fraction of the viral diversity, accounting for 1678 scaffolds. Of these, 53 had a CheckV completeness higher than 50%, and six contained terminal repeats. In total 243 exceeded 10 kb,

which likely represent near-complete genomes, as their length is typically around 20 kb^{33,34}. PLVs also constitute a significant proportion of reads, averaging 3.5% and 1.2% of cellular and viral fractions respectively (Fig. 1d, e). A maximum of 27% of the viral reads in the cellular fraction during January 2019 probably reflects an increase in the cellular host abundance rather than lytic viral infection, as these are prevalent endogenous viral elements of eukaryotes³³. Meanwhile, their abundance and detection in the viral fraction likely indicates a shift to an active infectious state.

Though the used standard Illumina library preparation method is biased against ssDNA viruses³⁵, we identified five scaffolds assigned to the *Microviridae* family (non-enveloped bacteriophages), two belonging to the filamentous *Inoviridae* family (both infecting bacteria), and 16 to the eukaryotic specific *Circoviridae* family³⁶. We do not expect ssDNA viruses to be a significant portion of the DNA viral communities, as previous surveys using methods biased towards ssDNA viruses still found dsDNA viruses to dominate²⁸.

Antarctic virus diversity responds to seasonal changes

Viral communities changed over the sampling period and could be delineated into four distinct clusters (Fig. 2a, b), each representing specific periods in the productive season (November to March) with distinct environmental conditions. The early summer (cluster D) is characterized by low water temperature, high salinity, high dissolved inorganic nutrient concentrations, low chlorophyll a (Chl-a) concentration, and low bacterial and viral abundances. During mid-summer (cluster A), increased temperature led to sea-ice melting and subsequently lower salinity and stronger stratification (shallower mixed layer depth). Accordingly, higher photosynthetic active radiation (PAR) coincided with peak Chl-a concentrations and nutrient depletion, while bacterial and viral abundances increased. Late-summer (cluster C) showed reducing Chl-a concentrations and prokaryote abundance and the peak in viral abundance. This cluster also coincided with increased temperature, diminished sea-ice cover, and relatively low nutrients. By the onset of autumn (cluster B), higher wind activity and lowered temperature led to increased mixing and sea-ice formation (with replenished nutrient concentrations and increased salinity) and declining microbial productivity (low Chl-a and microbial abundances)³⁷. February 2018 and 2019 came in two separate clusters (C and A respectively), indicating some interannual variability.

We evaluated environmental determinants of virus community composition using a multivariate regression model. Temperature and salinity explained 31% of the community variance (p -value = 0.001 and 0.004, respectively), while another 23% was explained by inorganic phosphate (p -value = 0.001), nitrogen-to-phosphorus ratio (p -value = 0.016), and PAR (p -value = 0.077). The correlation between viral and microbial community compositions (Supplementary Fig. 3) was examined by comparing the pairwise-Aitchison distances. The overall Microbial community composition explained 68% of the variation in the viral community when controlling for the environmental variables (partial Mantel r -statistic = 0.6842, p -value = 0.01). Meanwhile, for the prokaryotic community composition and phage community alone the partial Mantel r -statistic was 0.3411 with a p -value of 0.002.

The abundances and temporal dynamics of the dominant viruses mirrored the total virus count by flow cytometry (Fig. 2c; $R^2 = 0.82$ and p -value = 9.5×10^{-7}), and followed the bacterial (bloom) dynamics (Fig. 3a). Viral communities in late summer were directed by a higher contribution (and number) of the dominant viruses (96% *Caudoviricetes*; Supplementary data 1) than in November to mid-January (Fig. 2c). Consequently, during periods of high viral abundance, the viral communities were heavily skewed towards this small subset of viruses, leading to a decrease in alpha diversity (Fig. 2d and Supplementary Fig. 2c–e). Overall, these results highlight distinct viral communities during different periods in the season (Fig. 2c).

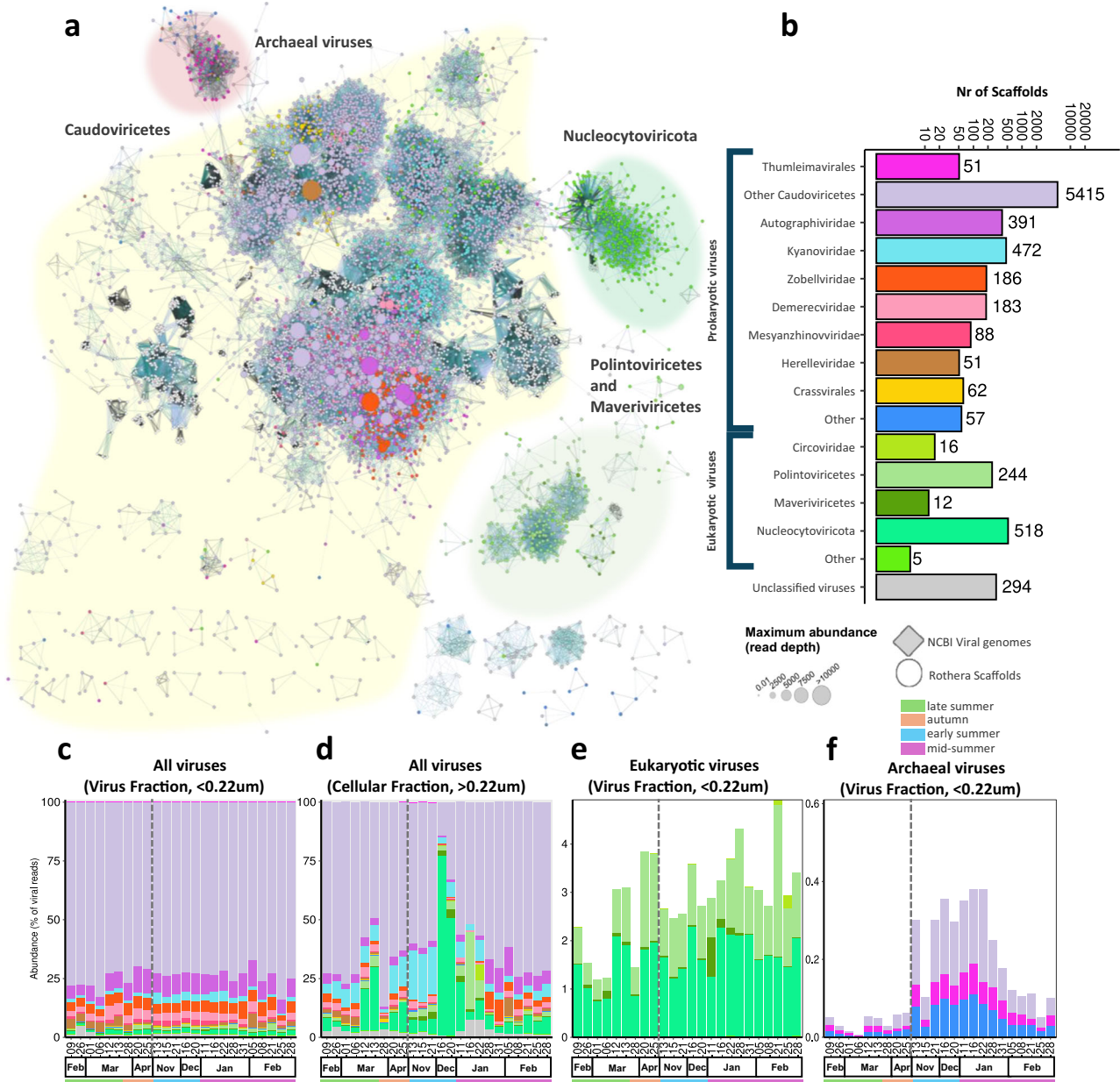


Fig. 1 | Taxonomic diversity of Antarctic dsDNA viruses over the productive season. **a** Gene sharing network of mid to high-quality viral contigs (>10 kb or 70% complete) coloured by taxonomic classification (see panel **b** for legend). The node size represents the maximum read abundance over the whole virome dataset. The shaded cluster was determined manually by overlaying the cenote-taker2 taxonomy. Family level taxonomy for *Caudoviricetes* predicted using PhaGCN2. *Nucleocyotiviricota*, *Maveriviricetes*, *Polintoviricetes*, and *Crassvirales* were classified with a costume approach. **b** Number of scaffolds classified to each taxonomic

rank (other represents ranks with less than 50 scaffolds). **c–f** Read abundance for viral taxa, reads were mapped to all scaffolds and abundance normalized to the total viral reads for all viruses in the viral fraction (<0.22 μm) (**c**) and cellular fraction (>0.22 μm) (**d**) and for archaeal viruses (**f**) and eukaryotic viruses (**e**) in the viral fraction (<0.22 μm). Note that the are compositional and the total virus particle abundances (Fig. 3c). The dashed vertical line indicates the winter sampling gap between April and November 2018.

Abundant Antarctic bacteriophages infect co-abundant bacterial taxa

We predicted the hosts of 2412 viral scaffolds using the integrated bacteriophage host prediction tool iPhoP³⁸. These scaffolds covered 48% of the reads mapping to mid to high-quality bacteriophage genomes (Fig. 3d) and were consistent with the vContact2 gene-sharing network analysis (Supplementary Fig. 4). Most bacteriophages targeted one of the three predominant bacterial classes (Fig. 3): *Gammaproteobacteria* (n=769), *Flavobacteria* (n=545), and *Alphaproteobacteria* (n=348), which are important components of coastal Antarctic bacterial communities^{39–41}. iPhoP predicted 59

viruses to infect Archaea which peaked in February (Fig. 3c), contrasting with the seasonal abundance of Archaea (Fig. 3a) and archaeal cluster viruses (Fig. 1e).

Gammaproteobacteria-infecting bacteriophages represented 25% of the dominant phages (Supplementary data 1), suggesting a significant role in seasonal virus production. In December, there was a noticeable rise in *Gammaproteobacteria*, predominantly *Oceanospirillales*, ahead of their bacteriophages (Fig. 3b–d). In late-summer (March), *Gammaproteobacteria* bacteriophage abundances were relatively high and increasing, while host abundances were not particularly high (Fig. 3d). In contrast, *Flavobacteria*-infecting bacteriophages

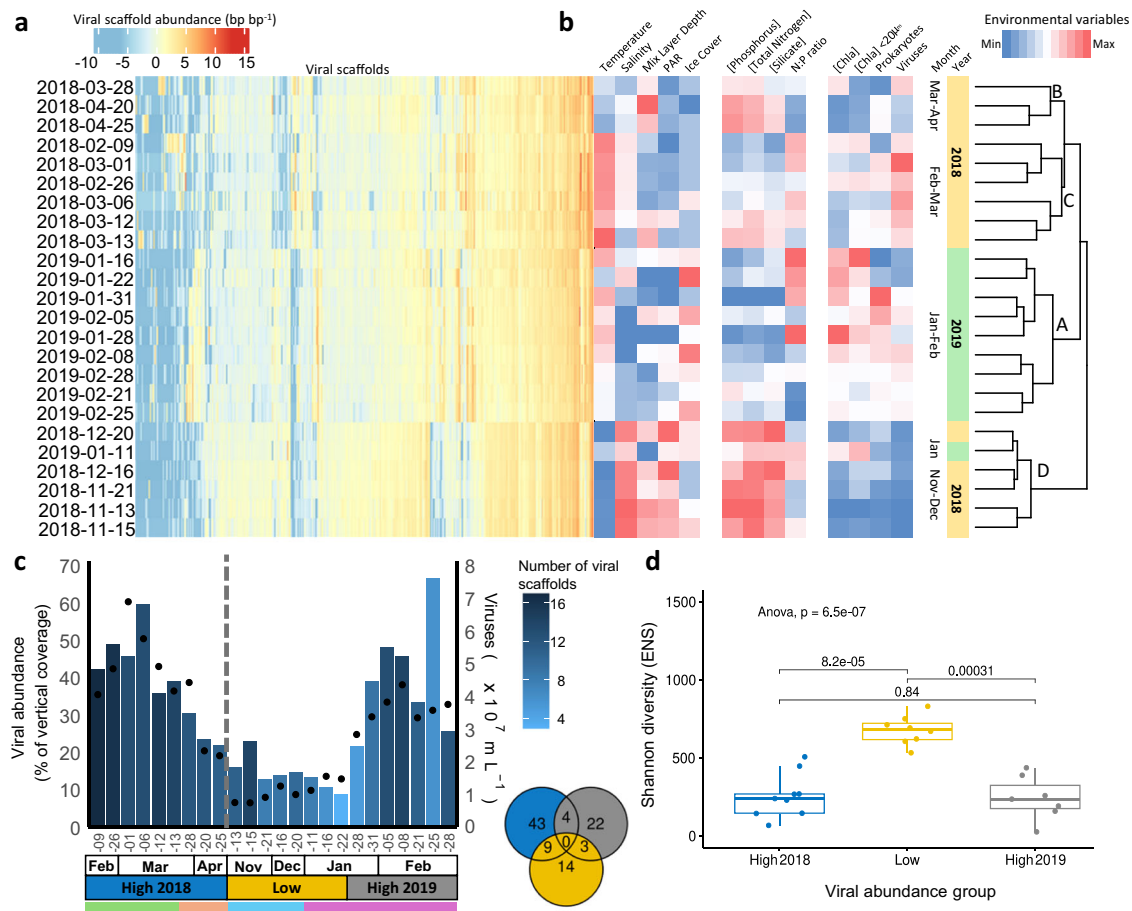


Fig. 2 | Seasonal dynamics of viral diversity. **a** Heatmap per sampling day of the clr -transformed scaffold vertical coverage (read abundance normalised by scaffold length) for mid to high quality scaffolds (>10 kb or 70% complete). **b** changes of relevant environmental variables, including temperature, salinity, mix layer depth, photosynthetic active radiation (PAR), ice cover for physical variables, phosphorus, total nitrogen, silicate, and nitrogen to phosphorus ratio (N:P ratio) for chemical variables, and total Chlorophyll a (Chl-a), $<20\ \mu\text{m}$ Chlorophyll a, prokaryotic cell counts, and viral particle counts for biological variables. The heatmap (**a**, **b**) are sorted vertically according to the hierarchical clustering of the clr -transformed viral abundances (dendrogram on the right). The letters on the dendrogram highlight the separate clusters referred to in the main text. **c** Compositional cumulative viral

vertical coverage of dominant viral scaffolds (with abundance $>0.1\%$) for mid to high quality scaffolds. Bar colours represent the number of dominant viral scaffolds per day and black dots represent the flow cytometry viral particle counts for the same day. The Venn diagram shows the number of shared and unique dominant viral scaffolds between different periods. The grey line indicates the winter sampling gap between April and November 2018. **d** Shannon diversity expressed in effective number of species (ENS) for the samples ($n = 24$) in the high and low viral-scaffold abundance periods (box plot represent median \pm quartiles and the whiskers the point range), these periods are denoted on (**c**), p -values for an ANOVA and pair-wise two-sided Wilcoxon tests are shown.

increased steadily with their host during December-January (mostly *Polaribacter*). *Alphaproteobacteria*-infecting bacteriophages were most abundant at the end of the season (April) and were still relatively high at the start of the next season (November), coinciding with the highest abundances of their predicted host (mostly SAR11). Thereafter, from December to January, the host population declined more rapidly than that of the bacteriophages.

Temperate bacteriophage reactivation with bacterial bloom onset

High prevalence of lysogenic infection has been reported throughout the Southern Ocean^{22,23,25}, and is potentially involved in the overwintering survival of Antarctic bacteriophages²³. To elucidate the seasonal dynamics of temperate bacteriophages, we monitored the abundance of viral scaffolds containing genes involved in lysogenization and prophage reactivation (Fig. 3e and Supplementary Fig. 5), specifically integrase ($n = 2502$), excisionase ($n = 40$), and bacteriophage repressor proteins ($n = 134$). Of the mid to high-quality phage sequences, 386 had at least one of the lysogeny genes. All genes displayed similar seasonal patterns in the cellular and viral fractions

(Supplementary Fig. 5). With an average vertical coverage (read abundance normalized by scaffold length) of $25,157\ \text{bp}\ \text{bp}^{-1}$, the scaffolds containing integrases were most abundant (2.4% of total viral vertical coverage). These viruses were most abundant during mid and late-summer (Supplementary Fig. 5), coinciding with elevated bacterial counts (Fig. 3a).

Antarctic waters harbor novel and diverse Crassvirales bacteriophages

Our target analysis identified 62 novel crassphage sequences (order *Crassvirales*). Of these, 17 were longer than 50 kb, 18 were at least 50% complete according to CheckV and seven had a completeness higher than 95%, two with direct terminal repeats. The terminase large subunit (TerL) phylogeny (Fig. 4a) validates the phylogenetic placement of these sequences within the *Crassvirales* order and their further classification at the family rank. Most scaffolds clustered into novel clades within the known *Crassvirales* diversity, labeled as C1 through C4 (Fig. 4a, b) and prospective new crassphage families. Additionally, 20 scaffolds belong to the *Steigviridae* family (Clade St, Fig. 4), which encompasses the *Cellulophaga* phage phi14:2 that infects marine free-

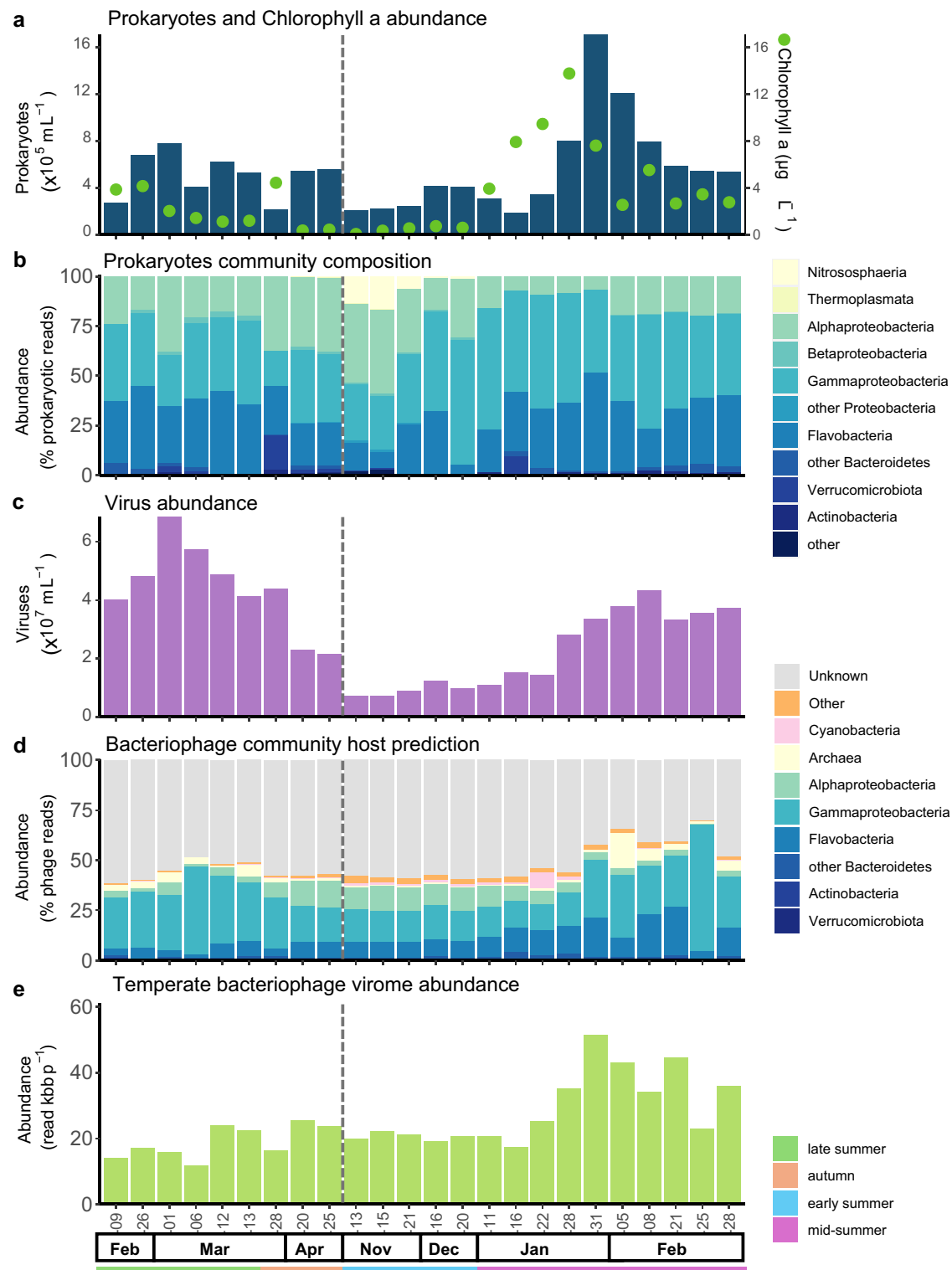


Fig. 3 | Bacteriophage and prokaryotic host dynamics. **a** Absolute prokaryotic abundances determined by flow cytometry, and chlorophyll a concentration. **b** Prokaryotic relative abundance (% of prokaryotic reads, $> 0.2 \mu\text{m}$) determined by PhyloFlash assembled 16S rRNA gene assembly at the class rank. **c** Absolute viral abundance determined by flow cytometry. **d** bacteriophage relative abundance (%)

of bacteriophage reads, $< 0.2 \mu\text{m}$) of mid to high-quality prokaryotic virus (longer than 10 kb or 70% complete) coloured according to the predicted host class. **e** abundance of viral scaffolds containing integrase expressed in vertical coverage (read bases per scaffold bases) for the viral fraction ($< 0.22 \mu\text{m}$). The grey dashed line indicates the winter sampling gap.

living *Flavobacteria*^{42,43}. We further confirmed the family placement with the phylogeny of the portal protein (Portal, $n = 51$) and major capsid protein (MCP, $n = 37$, Supplementary Fig. 6a, b). These crasphages presented a typical gene content and organization for members of the *Crassvirales* (Fig. 4c), with all the 30 core genes⁴⁴ identified

in at least one of the Antarctic *Crassvirales* scaffolds (Supplementary Fig. 6c). Clade C2 displayed the highest diversity and prevalence, with several viruses persisting throughout the season and others only detectable during autumn (April) and early summer (November to January).

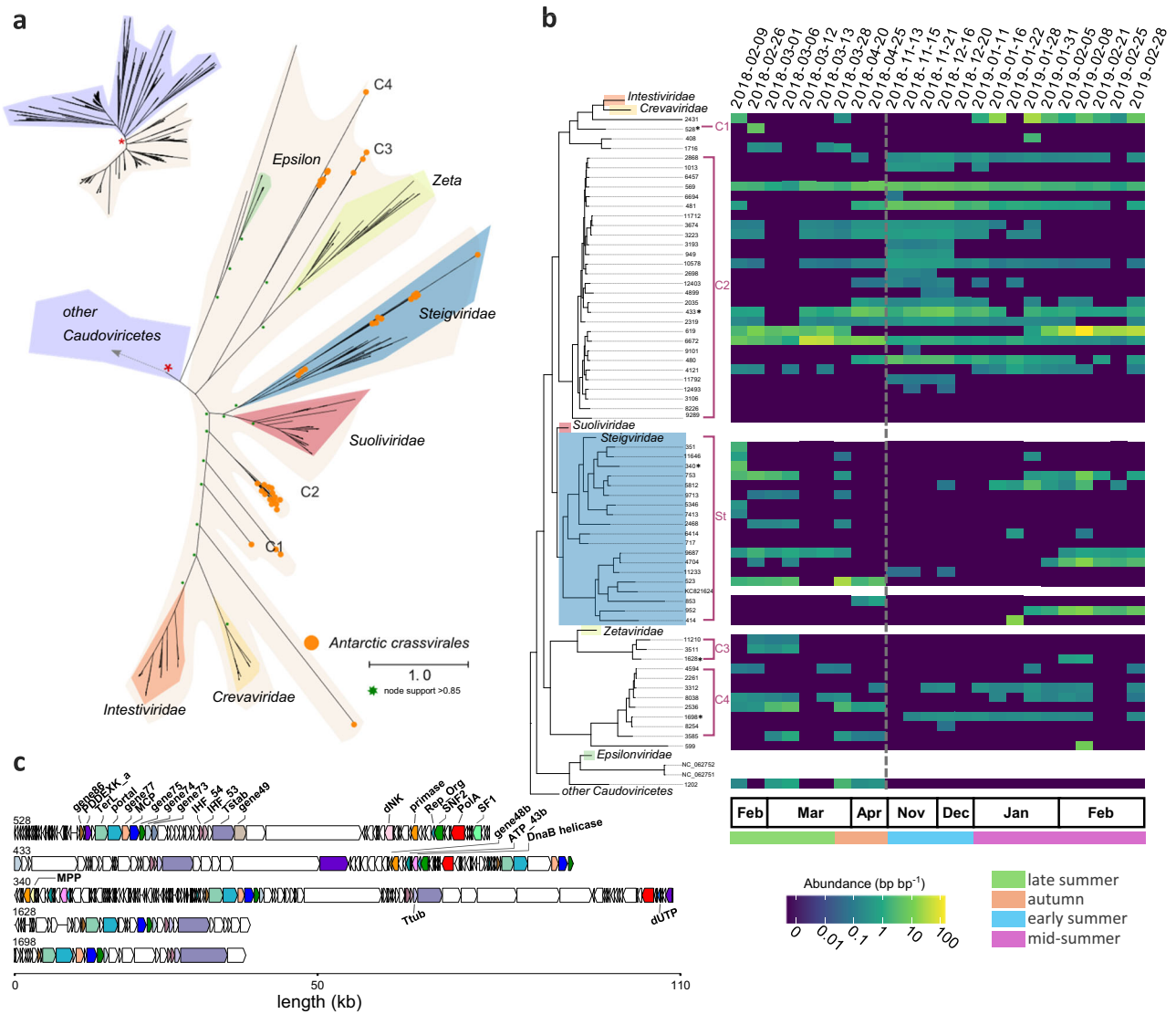


Fig. 4 | Diversity and dynamics of Antarctic Crassvirales. **a** Unrooted maximum likelihood phylogenetic tree of the terminase large subunit (TerL) of Antarctic Crassvirales scaffolds and reference crassviruses. Crassvirales found in this study are highlighted with the orange circles ($n = 62$) and shaded area corresponds to the Crassvirales order. **b** The Crassvirales section of the phylogenetic tree is shown on the left. Reference sequences from the five existing families have been collapsed, except for the Steigviridae that is interspersed with sequences from the Antarctic samples. The vertical coverage (read abundance normalised by scaffold length) for the viral fraction ($< 0.22 \mu\text{m}$) are shown as a heatmap. The grey dashed line indicates the winter sampling gap. **c** Genome map with functional gene annotations for

the longest crassviruses of each of the 5 clades, noted in (b) with *. The annotated genes are coloured consistently across the genome maps. Protein abbreviations as follows, major capsid protein (MCP), portal protein, putative structural proteins (genes 73–75, 77 and 86), integration host factor subunits (IHf 53 and 54), tail stabilization protein (Tstab), PD-(D/E)XK family nuclease (PDDEXK), crassvirus uncharacterized gene 49, DnaG family primase, replisome organizer protein (Rep_Org), SNF2 helicase, DNA polymerase family A (PolA), SFI helicase, AAA domain ATPase (ATP_43b), phage replicative helicase (DnaB), metallophosphatase (MPP), tail tubular protein (Ttub), dUTPase (dUTP).

Nucleocytoviricota viruses are a diverse and abundant group of Antarctic eukaryotic viruses

Considering the large genomes and particle sizes of many NCVs⁴⁵, we characterized their diversity using metagenomic binning in both the viral and cellular fractions. This resulted in 88 bins (Fig. 5a, Supplementary data 2), that were phylogenetically placed in the orders *Imitervirales* ($n = 51$), *Algavirales* ($n = 15$), candidate *Pandoravirales*¹⁶ ($n = 4$) and *Pimascovirales* ($n = 4$), and candidate class *Mriyaviricetes*⁴⁷ ($n = 9$). Additionally, our analysis recovered five bins belonging to the candidate phylum *Mirusviricota*, which shares some phylogenetic marker genes with NCVs⁴⁸.

Most *Imitervirales* bins belonged to the *Mesomimiviridae* family ($n = 25$), of which five belonged to the genus *Tethysvirus* which includes viruses infecting the prymnesiophytes *Phaeocystis globosa* and

Chrysochromulina ericina^{49,50}. The December peak of one prevalent Tethysvirus (Fig. 5b, c), coincided with a decline in *P. antarctica* (Supplementary Fig. 3c), the most abundant prymnesiophyte ($> 99\%$ of *Prymnesiophyceae* rRNA gene reads, except on 9 February and 6 March 2018). Of these, bin 2-643264.cc.b128 was the most abundant of all NCVs and closely related to *P. globosa* viruses. Twenty of the remaining *Imitervirales*-related bins belonged to the *Schizomimiviridae* family, with their peak abundance during late summer (Fig. 5b), particularly in the viral fraction (Supplementary Fig. 7). The remaining six *Imitervirales* viruses belonged to the *Allomimiviridae* family and occurred in late-summer (Feb-March; Fig. 5b, c).

Most *Algavirales* viruses belonged to the candidate family *Prasinoviridae* AG_01 ($n = 10$), of which six belonged to genus *Prasinovirus*. Additionally, one belonged to family AG_3 and three to AG_04

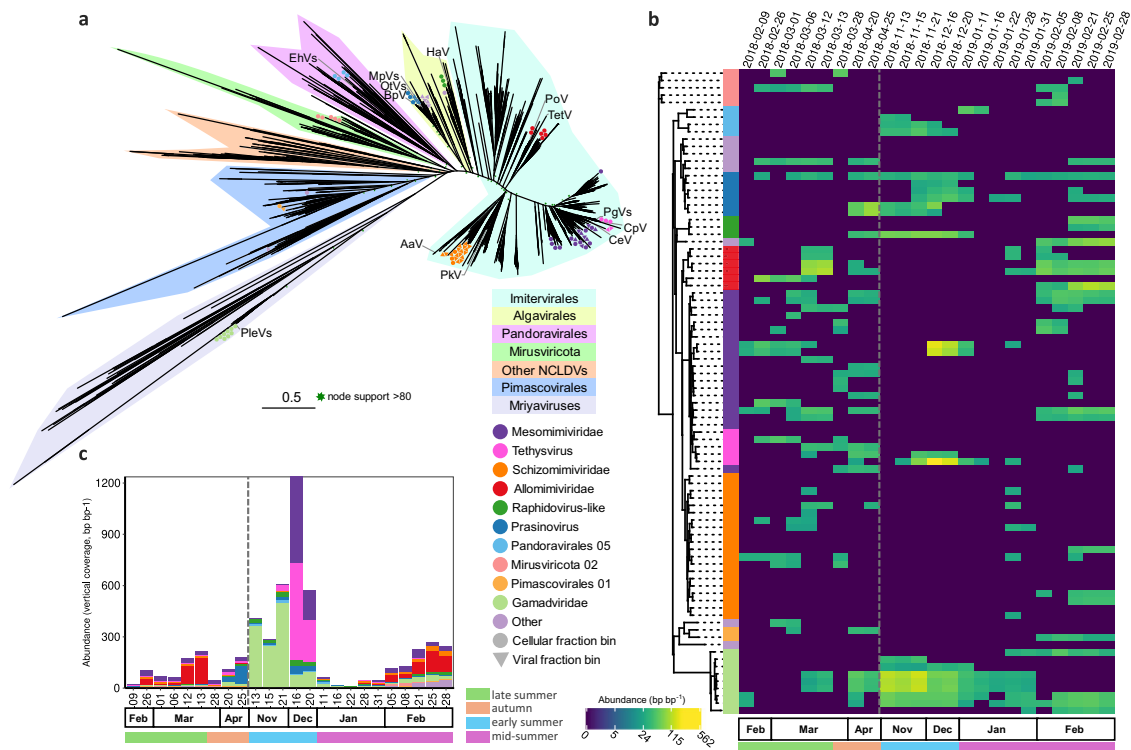


Fig. 5 | Diversity and seasonal dynamics of Antarctic NCVs. a Unrooted maximum likelihood phylogenetic tree of Antarctic NCVs, *Mirusviricota* and reference genomes from isolates and marine metagenomic surveys based on 7 concatenated marker genes. **b** Temporal dynamics of sequencing vertical abundance (read abundance normalised by bin length, log-scaled) for the cellular fraction metagenomes (>0.22 μm). The heatmap is organized phylogenetically (rooted between mirusviruses and NCVs) and the first column represents the taxonomy (see panel a). **c** temporal dynamics at the family level for the cellular fraction metagenomes in bin

vertical coverage (read abundance normalised by bin length). The grey dash line indicates the winter sampling gap between April and November 2018. Virus abbreviations are as follows, *Phaeocystis globosa* viruses (PgvVs), *Chrysochromulina ericina* and *C. parva* viruses (CeV and CpV), *Prymnesium kappa* virus (PkV), *Pyramimonas orientalis* virus (PoV) *Tetraselmis* sp. Virus (TetV), *Heterosigma akashiwo* virus (HaV), *Bathycoccus prasinos* (BpV), *Ostreococcus tauri* (OtV), *Micromonas pusilla* virus (MpV), *Aureococcus anophagefferens* virus (AaV) and *Emiliania huxleyi* viruses (EhVs).

(*Raphidovirus-like*), which were predominantly abundant in the cellular fraction during the autumn and early and mid-summer (Fig. 5b, c). Prasinovirus bin vRhyme.bin.4783 and AG_01 bin vRhyme.bin.4827 were persistent throughout the productive season in the viral fraction (Supplementary Fig. 7).

The nine Mriyaviruses all belong to the candidate family Gamadviridae and were found inserted into larger bins recovered from the cellular fraction. Eight of these bins had high Eukaryotic content, representing two unclassified Eukaryotes and six classified as *Phaeocystis antarctica* (Supplementary data 2). We hypothesize that these viruses were binned together with their host, representing temperate or persistent infection (Supplementary data 2), consistent with their presence inside the genome assemblies of *Phaeocystis*⁵¹ and other eukaryotes⁴⁷. Additionally, five bins in the candidate phylum *Mirusviricota*⁴⁸ were identified in the cellular fraction (Fig. 5b, c). Lastly, we detected eight NCVs of which four belonged to the order of the *Pimascovirales* (which includes the genera *Pithovirus*, and *Marseillevirus*) and four to the proposed *Pandoravirales*⁴⁶. The cellular fraction NCV composition co-varied with the Eukaryotic composition (partial Mantel r-statistic 0.2888, p -value 0.001), while controlling for environmental variables.

Antarctic virophages and polinton-like viruses expand the known diversity of these groups

By targeting their distinct yet diverse⁵² MCP phylogeny, we identified 1678 PLV and 57 virophage scaffolds, and delineated them at the family rank. Most PLVs and virophages possessed virus hallmarks other than MCP, e.g., packaging ATPase or one replication related gene such as

polymerase B, primase-helicase, or helicase (Fig. 6c, d). Their gene-sharing network clustering agrees with the MCP clades (Supplementary Fig. 8), while viruses of the *Omnimimiviridae* seem to share more genes with TsV and PgvV group PLVs than with other virophages. Similarly, Chi group PLVs seem to share more genes with virophages than with other PLVs, reflecting their complex evolutionary relationships⁵³.

For the virophages, we applied the recently updated taxonomic framework⁵². Most sequences belonged to the families *Sputniviroidae* ($n=13$), and *Omnimimiviridae* ($n=12$). The most abundant virophage (NODE_23824) belonged to the latter family and is closely related to the Antarctic organic lake virophage⁵⁴. Notably, a distinct MCP clade of 30 virophages was identified, likely forming a novel virophage family (Fig. 6a). Within this clade, the virophage sequence NODE_3533 has a presumably complete 23.9 kb genome with core genes and direct terminal repeats (Fig. 6c). This sequence occurred mostly in January, together with NODE_23824, whereas NODE_6367 and _4538 were most prevalent in March. Only NODE_29197 dominated at the start and end of the season.

We identified NCVs putatively associated with these virophages by matching the promoter motif of the virophages with the late transcription promoter motifs of the co-occurring NCVs (Supplementary data 3 and Fig. 6c), as these are often shared^{55,56}. Antarctic virophages from the *Sputniviroidae* matched with two mesomimiviruses, and a schizomimivirus. In the *Omnimimiviridae*, one matched with mesomimivirus, and two with prasinoviruses. The novel clade matched mostly with prasinoviruses, and mesomimiviruses with one match to a schizomimivirus, a mirusvirus, and a pandoravirus.

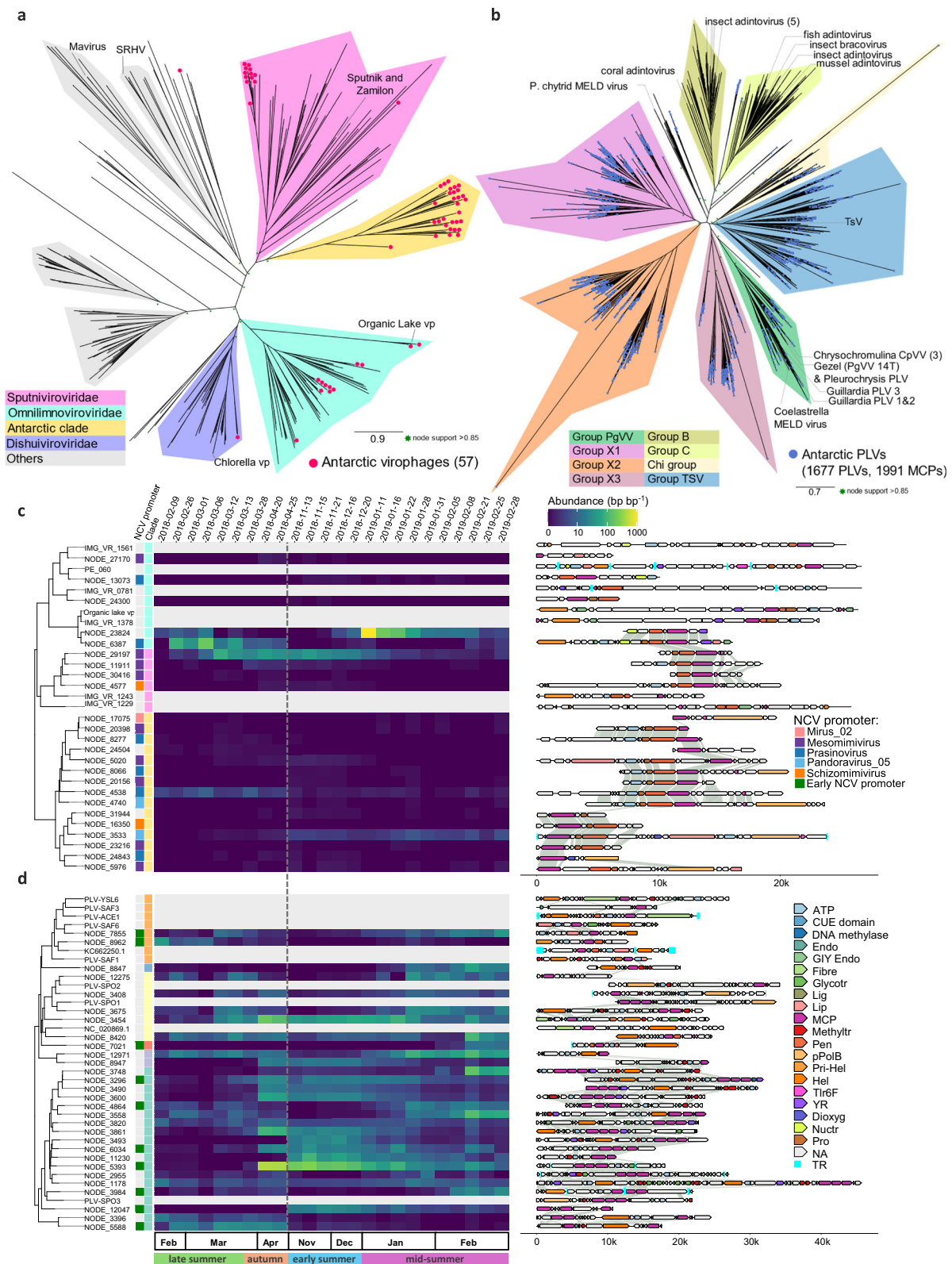


Fig. 6 | Antarctic virophages and polinton-like viruses. Shown are major capsid protein (MCP) phylogenies for (a) virophages (vp, *Maveriviricetes*) and (b) polinton-like viruses (PLV, *Polintoviricetes*). Virophage family and PLV clade names according to refs. 29,37,38. Phylogeny for (c) virophages longer than 5 kb and (d) top 30 most abundant PLVs longer than 10 kb with the corresponding heatmap of meta-genome abundance in the viral fraction (< 0.22 μm) and annotated genome map. Protein abbreviations as follows, FtsK-HerA family DNA-packaging ATPase (ATP),

dioxygenase (Dioxyg), endonuclease (Endo), GIY-YIG nuclease domains (GIY), fibre-like protein (Fibre), glycosyltransferase (Glycotr), ligase (Lig), lipase (Lip), methyltransferase (Methyltr), nucleotidyltransferase (Nuctr), penton (Pen), protein-primed polymerase B (pPolB), primase-helicase (Prim-Hel), helicase (Hel), maturation Cysteine Protease (Pro), uncharacterized protein (Tlr6F), putative tyrosine recombinase (YR). The dash grey line indicates the winter sampling gap.

We classified PLVs based on previous surveys on this group^{34,57}, as most clades have no formal taxonomic classification. Remarkably, Antarctic PLVs populated most MCP phylogenetic groups (Fig. 6b), except for clades A and B which mostly contain MCPs endogenous to Opisthokonta genomes, and animal adintoviruses (Fig. 6b). Another three separate groups (X1, X2, and X3) could be defined, with reference viruses from the previous clade X⁴⁰ and cluster TriMCP⁵⁷. These groups seem to arise from single PLVs exhibiting a highly divergent MCP gene triplication (Fig. 6b and Supplementary Fig. 9a). MCPs from the same PLV are generally more closely related in TSV than in group X, with their phylogenetic distance being on average 2.4 times greater than in group X (p -value < 2.2E-16, t -test). Additionally, this distance is on average 2.26 times smaller than between MCPs from different PLVs in the TsV group (p -value < 2.2E-16, t -test). In group X, shorter sequences with less than three MCPs are likely incomplete (Supplementary Fig. 9). Many of these PLVs MCP ($n = 1387$) make-up novel clades within these three groups. Most of the 291 remaining Antarctic PLVs belong to the Chi, TsV, and PgVV groups, with several forming distinct Antarctic clades (Fig. 6b). Of the 30 most abundant PLVs (>10 kb), about half were prevalent during February, and the others during the autumn and early summer (Fig. 6d). We investigated the possibility of these viruses parasitizing on NCVs by matching their promoter motif with the NCV early transcription promoter motif 'WWWWWTGWWWW', as was found for Gezel-14T (Supplementary data 3 and Fig. 6d). This resulted in matches for 19% of the clade PgVV, 11% of the clades X1-3 and Chi and 6% of the clade TsV longer than 5 kb.

Discussion

This study provides an in-depth characterization of highly unique marine DNA viral diversity in Antarctic surface waters, where 75% of viral species were not present in the GOV⁸ and SOV²⁹ datasets. The limited overlap with SOV indicates a high degree of variability within the Antarctic virome. Overall, these findings underscore the Southern Ocean as an underexplored region regarding viral diversity, emphasizing the need for further comprehensive studies in this region. Beyond identifying a high proportion of new viral species, our comprehensive approach uncovered novel diversity at higher taxonomic ranks. The discovery of four novel *Crassvirales* families, C2 and C4 with many representatives greatly expands our understanding of crassphage diversity, and their environmental range, beyond the primate gut microbiome^{43,58}. The new-found diversity of crassphages in the Antarctic calls for further investigation of this class regarding diversity and activity in both the marine and other non-host-associated environments. Mining public data repositories may reveal additional members of these newly discovered lineages. These viruses might similarly⁵⁹ infect Antarctic *Bacteroidetes*, a significant component of Marguerite Bay bacterial communities (classes *Flavobacteria*, *Sphingobacteriia*, *Saprospiria* and *Cytophagia*). Similarly, we discovered a novel virophage family and successfully recovered a complete genome of this family. Virophages replicate with co-infecting NCVs and may, in some cases such as mavirus, provide their hosts' population-level protection against NCVs^{60,61}. Since virophages parasitize the transcription machinery of their associated NCVs, the gene promoter motifs between giant viruses and virophages often share detectable similarity. In our analysis, we attempted to match virophages to their co-occurring NCVs by their putative promoters. Surprisingly, we found promoter signals that were shared between virophage and prasinovirus sequences, suggesting that virophages can depend on NCVs outside the *Imitervirales* order⁵². Our findings reveal a remarkably high diversity of PLVs, a highly understudied group^{34,57} that was recently found prevalent in Eukaryotic genomes³³. The notable prominence of PLVs in our dataset (1,678 sequences) raises the question of whether this is Antarctic-specific or more widespread in the ocean, as has been found for freshwater environments⁵⁷. We found 154 PgVV-clade PLVs³⁴, with the one known isolate displaying a virophage-like lifestyle (Gezel-

14T⁵¹). These PLVs had the highest proportion of matches to the NCV early transcription promoter motif, suggesting that, similarly to Gezel-14T, they may also depend on NCVs. While five sequences related to Gezel-14T have been previously reported in Antarctic virome samples²⁷, our study substantially broadens the known diversity of Antarctic PLVs beyond the PgVV group. Additionally, 360 PLVs belonged to the TsV group that includes PLV *Tetraselmis viridis* virus S1 that does not require an NCV co-infection⁶². Notably, most PLVs (1387) were related to those in group X³⁴ which our analysis shows to form three MCP clades, many representing one virus with duplicate and triplicate MCPs. The high divergence between the group X MCPs suggests this to be an early evolutionary event, contrasting with the triplication in group TsV which tends to have more closely related triplicates. In summary, these findings paint a picture of PLVs as an active and diverse group of viruses infecting Antarctic eukaryotes.

Another highlight of this study is the improved insight into the intricate relationship between host and virus. The NCVs were the dominant eukaryotic viruses and most belonged to the families *Allo-*, *Meso-*, and *Schizomimiviridae*, as well as the order *Algavirales*, of which all isolated members infect photosynthetic protists. The prevalence and temporal dynamics of these NCVs reinforces their active role in affecting Antarctic phytoplankton population dynamics^{24,26}, ranging from preventive to reductive viral control⁶³. Indeed, some of the prasinoviruses, for which all isolates are known to infect picophytoplankton in the order *Mamiellales*⁶⁴, and capable of maintaining stable coexistence with their hosts⁶⁵, were remarkably persistent suggesting a more continuous lysis pressure. PgV-like viruses from the genus *Tethysvirus* have previously been identified as an important member of Antarctic viral communities^{27,66}. Our study's temporal resolution sheds light on their role in impacting bloom decline of the co-occurring *P. antarctica* host (reductive control), aligning with recent findings of viral lysis being a major mortality factor of this Antarctic phytoplankton²⁴. The steep increase in PgV-like viruses at the end of a *P. antarctica* bloom in December corresponded with the increase of *Gammaproteobacteria*. This bacterial group has been reported to quickly respond to viral infection of *Phaeocystis*⁶⁷, reinforcing the importance of viral lysis in fueling the microbial loop. Overall, this study provides a comprehensive characterization of the *Bamfordvirae* kingdom diversity at the study site. This characterization expands the known PLV and virophage diversity, includes the recovery of novel NCVs together with those belonging to the candidate class *Mriyaviricetes*⁴⁷, and also identifies members of the recently described candidate phylum *Mirusviricota*⁴⁸.

The comprehensive seasonal coverage and enhanced sampling resolution of this study reveals that timing of sampling affects the likelihood of virus detection and discovery. Temporal sampling improves the understanding of the dynamics of the different viruses, i.e., NCVs, virophages, PLVs and phages in our study. It offered a deeper insight into prokaryotic bacteriophage-host interactions, with group-specific responses. For instance, *Gammaproteobacteria* displayed a typical predator-prey relationship illustrated by the decoupling between the host and bacteriophages abundance during the low sea-ice period. This pattern, characterized by high viral activity and low host abundance, was also found by viral activity assays in the ice-free areas of the Weddell Sea²². Such observations gain significance in the context of global warming, which is leading to the expansion of ice-free zones and longer ice-free periods around the Antarctic Peninsula⁶⁸. Moreover, we found closely coupled dynamics of *Flavobacteria* with their bacteriophages, particularly during the phytoplankton bloom in January (cluster A). The increasing abundance of *Flavobacteria* bacteriophages coincided with the bacterial bloom, whereas *Gammaproteobacteria* bacteriophages were most dominant after the bloom (cluster C). Such successional pattern can be explained by the association of Antarctic *Flavobacteria* with Chl-a fluorescence, and their degradation of diverse complex organic compounds^{69,70}.

They make labile compounds available to other bacteria such as the *Gammaproteobacteria* and *Alphaproteobacteria*⁶⁹. In our study, *Alphaproteobacteria* and their bacteriophages became more prominent during the colder periods, at the end of the season (cluster B) and pre-bloom phase (cluster D), consistent with this group's affinity with low temperature⁷¹.

The early summer marks an important transition for viral communities, where the onset of microbial production leads to increased bacteriophage production and abundance²⁵. Our analysis shows this period is characterized by the emergence of a few dominant bacteriophages that account for a substantial portion of viral activity. A pronounced increase in bacteriophage activity during these months in the same study area led to a shift in carbon flow towards the microbial loop rather than higher trophic levels²⁵. Concurrently, there is an apparent activation of temperate bacteriophages during the bacterial bloom, which is indicative of a refugium-to-activation dynamics⁷², and aligns with earlier research focusing on Antarctic prophage induction^{22,23,25}.

This study reports for the first time the strong seasonal variations in diversity and dynamics for the Antarctic viral community. Our phylogeny-informed characterization of viral diversity underscores the distinctness of these communities. Finally, the time-resolved and co-sampling of host communities offers a unique perspective, shedding light on the seasonality and abundance of Antarctic marine viruses and providing a more complete understanding of their diversity in relation to microbial hosts.

Methods

Study site and sample collection

Samples were collected from 15 m depth in Marguerite Bay at the site of the Rothera Time-Series⁷³ (RaTS, latitude 67.572°S; longitude 68.231°W). Sampling conditions in the Antarctic are highly variable and not always favorable for sampling, still we were able to collect samples on 24 days over two consecutive productive seasons (seven months period, from February until April 2018 and from November 2018 until February 2019). The water column properties were characterized using a SeaBird SBE 19 + CTD that measured conductivity, temperature, depth, salinity, chlorophyll autofluorescence, and photosynthetically available radiation. Mix layer depth (MLD) was defined as the depth with a water density difference of 0.05 kg m⁻³ relative to the surface¹⁹. Water samples were collected by performing sequential casts with Niskin bottles. These were emptied by gentle siphoning (using clean PC tube) into 20 L pre-rinsed polycarbonate carboys. All carboys and tubing used for sampling were decontaminated by rinsing with Contrad 70™ 2% v/v, followed by MilliQ ultrapure water (UP). Prior to sample collection, carboys were rinsed thrice with sample water. The carboys were protected from direct sunlight using opaque bags. Sampling was performed in the morning between 9:30 and 11:00 AM. Samples were further processed within 4 h from the start of sampling. The lab was kept at in situ temperature (with a minimum of 0.1 °C), and if needed, samples were kept on ice.

For dissolved inorganic nutrient subsampling, seawater was filtered through a 0.2 µm pore-size Supor membrane Acrodisc® filter (Pall, Port Washington, NY 11050, USA) and collected in 3 times sample-rinsed high-density polyethylene pony vials (PerkinElmer, USA). The subsamples for dissolved inorganic nitrogen and phosphorus were stored at -20 °C until analysis, and samples for dissolved inorganic silicate were stored in the dark at 4 °C. Samples for chlorophyll-a (Chl-a) were collected by filtering 1 to 8.5 L of unfiltered (total Chl-a) and 20 µm reverse-sieved (<20 µm fraction) onto GF/F filters (Whatman, UK), after which the filters were each wrapped in aluminum-foil, placed in a plastic bag, flash-frozen in liquid nitrogen, and stored at -80 °C until further analysis. For microbial abundances, 1 mL of seawater was fixed with glutaraldehyde to 0.5% v/v final concentration (25%, EM-grade, Sigma Aldrich, USA) for 30 min at 1 °C (in

the dark), after which it was flash-frozen in liquid nitrogen and stored at -80 °C until analysis in the NIOZ laboratory (The Netherlands). Phytoplankton cells were counted on fresh samples (kept on ice) directly upon arrival in the Rothera lab.

Prior to handling the genomic samples, all bench surfaces were cleaned with Contrad 70™ 2% v/v (Decon Labs, East Sussex, UK) and rinsed with UP water. The cellular fraction metagenomic samples were collected by filtering 3 to 15 L (1 h filtering time at in situ temperature) of whole water through a 0.22 µm Sterivex™ (MilliporeSigma, Massachusetts, US). The filters were sealed with parafilm and stored at -80 °C until extraction. The viral fraction metagenomic samples were collected from 20 L seawater using the iron flocculation method according to Hurwitz et al. 2013 (ref. 74). Briefly, particles bigger than 0.22 µm were removed by two sequential filtrations using a A/E glass fiber filter (142 mm, Whatman, GE Healthcare, UK) followed by a 0.22 µm PES filter (142 mm, MilliporeSigma, Massachusetts, US). The viruses were flocculated with 1 mg L⁻¹ of FeCl₃ (1 h incubation) and collected onto a 1 µm PC filter (142 mm, Whatman, GE Healthcare, UK). Filters were stored at 4 °C in the dark until further analysis. The full sampling metadata is available in Supplementary data 4.

Microbial abundances, chlorophyll-a, and nutrient concentrations

Viruses and bacteria were enumerated according to Brussaard et al. (2010, ref. 75) with modification to the TE-buffer (pH 8.2, according to ref. 76). Upon dilution in TE-buffer and staining with SYBRGreen-I (Sigma Aldrich, USA), the samples were enumerated using a FACSCalibur flow cytometer (BD Biosciences, USA) equipped with an air-cooled Argon laser with an excitation wavelength of 488 nm with the trigger on green fluorescence (Supplementary Fig. 10). Total phytoplankton abundances were obtained using a benchtop FACS Celesta flow cytometer (BD Biosciences, USA) with the trigger on red chlorophyll autofluorescence⁷⁷.

Chlorophyll-a concentration (Chl-a) was determined using HPLC (according to ref. 18). Briefly, filters were freeze dried (48 h) and pigments were extracted using 90% acetone (48 h at 4 °C in the dark)⁷⁸. Pigments were separated by high performance liquid chromatography (HPLC; Waters model 2690), equipped with a 3.5 µm particle size Zorbax Eclipse XDB-C8 column with a cooled autosampler (4 °C) according to Van Heukelem and Thomas (2001). Pigment detection and quantification was based on comparison with DHI LAB standards at 346 nm (Waters 996 HPLC Photodiode Array Detector)⁷⁹.

The concentrations of dissolved inorganic macro-nutrients were obtained using a TRAACS 800 autoanalyzer (Bran+Luebbe, Germany), following Grasshoff et al. (1983) for nitrate and nitrite, of Murphy and Riley (1962) for phosphate, and of Strickland and Parsons (1968) for silicate (refs. 80–82). The calibration standards were diluted in low nutrient seawater (LNSW) with salinity levels similar to the samples (35‰). The detection limit was 0.007 µM for nitrate + nitrite, 0.001 µM for nitrite, 0.007 µM for phosphate, and 0.03 µM for silicate.

Viral and cellular fraction metagenomes

The DNA of the cellular fraction (Sterivex filters) was extracted using the Qiagen DNeasy Powersoil kit (Qiagen, Carlsbad, USA), according to the manufacturer's instructions. The filters were opened and cut into approximately 3 × 3 mm pieces prior to 2 × 10 s bead beating at 3.55 m s⁻¹ with a 30 sec dwell on a Bead Ruptor Elite (Omni International, USA). Viruses from the viral fraction (iron flocculation method) were resuspended at 4 °C overnight in a EDTA (0.1 M) - MgCl₂ (0.2 M) - ascorbate (0.2 M) buffer with pH of 6.0 (1 mL per liter of sampled seawater). The resuspended sample was gently filtered through a 0.45 µm SFCA syringe filter (Sartorius, Göttingen, Germany) and treated with 1 U µL⁻¹ of DNase I (Roche, Basel, Switzerland) for 18 h at 4 °C. DNase I was deactivated by adding EDTA and EGTA (0.1 M final concentration). The viruses were concentrated to a volume of 0.8 to 1 mL

using a 100 kDa Amicon (MilliporeSigma, Massachusetts, US). DNA was extracted using Wizard® PCR Preps DNA Purification kit (Promega, Wisconsin, United States) according to manufacturer's instructions. The DNA was eluted twice in 50 µL of 80 °C molecular grade low TE buffer (pH 8.0, 10 mM Tris and 0.1 mM EDTA).

The libraries were prepared using the TruSeq Nano DNA Kit (Illumina, San Diego, CA) and sequenced with the Illumina platform NovaSeq6000 S2 (2 × 150 bp), according to the manufacturer's instructions, on average 80 M reads per sample (58–123 M). The read quality was assessed before and after quality trimming using MultiQC v1.8⁸³. PhiX reads were removed using bbdut v38.07 (<https://sourceforge.net/projects/bbmap/>), low complexity (dust filter threshold of 20) and PCR duplicates were removed with prinseq-lite v0.20.4⁸⁴. Illumina adaptors were clipped with trimmomatic v0.36⁸⁵. To assess the degree of enrichment of our viromes, the abundance of microbial genetic markers was assessed using ViromeQC v1.0.1 in all metagenomes⁸⁶.

PhyloFlash v3.4⁸⁷ was used to characterize microbial communities by target assembly and classification of the 16/18S rRNA gene. Reads that mapped to plastid 16S rRNA genes were removed.

Virus genome assembly, taxonomy, and host prediction

All reads from the viral fraction metagenomes were co-assembled into scaffolds using metaSpades v3.14.1⁸⁸. Scaffolds of at least 1500 bp long were checked for viral signals using PPR-Meta v1.1⁸⁹, which was found to be the most sensitive virus prediction tool with relatively few false positives in a benchmark work that included some of the samples from this study⁹⁰. Sequences identified as viral but with no CheckV v0.7.0 viral hallmark genes and cellular hallmark genes³¹ and classified as non-viral by Cenote-Taker2²¹ were removed. The remaining co-assembled scaffolds are equivalent to viral species-level operational taxonomic units (vOTUS) as clustering at 95% identity over 85% of the sequences⁸ resulted in the clustering of only 0.039% of the sequences.

We quantified the overlap between Rothera viral sequences and the Global Ocean Virome⁸ and Southern Ocean Virome²⁹ datasets by performing an all versus all blastn which were then clustered at 95% average nucleotide identity over 80% of the sequence using the CheckV virus clustering.

For viral sequences longer than 5000 bp or with $\geq 70\%$ completeness (CheckV completeness), coding regions were predicted using prodigal⁹² (v2.6.3 -p meta). The viral sequences were clustered based on their coding regions using vContact2⁹³ using the RefSeq prokaryotic viruses (--db ProkaryoticViralRefSeq94-Merged) together with a custom collection of protist DNA viruses (Supplementary data 5). The clusters were visualized using Cytoscape v3.8.2 with a perforce force-directed layout⁹⁴, and scaffold viral taxonomy was overlaid. In the sections below we detail the target identification of *Crassvirales*, *Nucleocytoviricota* and *Preplasmiviricota* (PLVs and virophages), while for other viral sequences we used the Cenote-taker2 taxonomy. The *Caudoviricetes* (the single class in the *Uroviricota* Phylum), *Nucleocytoviricota*, *Preplasmiviricota*, and archaeal virus groups were manually defined (Supplementary Fig. 11) which always corresponded with the taxonomy of reference genomes within those groups and largely with the Cenote-taker2 taxonomy for the metagenomic viral sequences. Unknown sequences within the above defined groups were attributed the group phylum rank taxonomy. Scaffolds annotated as *Caudoviricetes* by Cenote-taker2 and all sequences within the *Caudoviricetes* mega cluster (excluding the archaeal group) were further classified into family rank taxonomy using PhaGCN2³². Archaeal group sequences classified as halovirus by cenote-taker were classified as *Thumleimavirales*. For *Crassvirales*, *Nucleocytoviricota*, *Maveriviricetes* (virophages) and *Polintoviricetes* (polinton-like viruses) sequences, we performed a targeted identification and taxonomic classification (see sections below).

The host genus was predicted for high and mid-quality bacteriophage sequences (longer than 10 kb or at least 70% complete) using iPhoP v0.9³⁸ with the standard cut-off for genus rank prediction and a 0.2 false discovery rate cut-off for class and phylum rank prediction (using All_combined_scores.csv). Conflicting host predictions were removed. The standard genus level output resulted in 744 predictions while the lower prediction threshold resulted in 1668 predictions at the class level.

All viral sequences, excluding those classified as eukaryotic viruses, were inspected for the presence of the lysogeny genes integrase, excisionase, and bacteriophage repressor protein. The coding regions were predicted using prodigal⁹² (v2.6.3 -p meta) which were matched by hmmsearch (e-value 1e-5, HMMER v3.1b2) to HMM profiles from the PFAM (34.0), KO (97.0), ncbi COGs (COGS2020) and by diamond search (e-value 1e-10, v0.9.22) to the nrNCBI (downloaded in March 2022). For integrase were considered matches to K03733, K14059, K04763, K21039, COG0582, COG1518, PF00589, PF13495, PF00665, PF13683, PF13102, PF18697, PF09003, PF02899, PF12835, PF02022, PF14659, PF18644, PF13976, PF13333, PF14882, PF12834, PF17921 and those containing the string "integrase" in the diamond top hit excluding those containing the string "CRISPR" and "Transposase". For excisionase were considered matches to PF06806 and PF0782, and those containing the string "excisionase" in the diamond top hit. For the phage repressor protein were considered matched to PF00717, K22300, K07727, K18830 and COG2932.

Reads from the viral and cellular metagenomes were mapped to all scaffolds using bwa v0.7.17 mem⁹⁵. Reads mapped with less than 95% identity over 80% of the read length were excluded with CoverM v0.6.1⁹⁶, and the number of reads mapped to each scaffold was calculated with samtools coverage v1.11⁹⁷. When scaffolds had less than 70% horizontal coverage, their abundance was set to 0. To remove the effect of non-viral contamination, the read relative abundances were calculated by dividing the read counts by the total number of viral reads in each sample. The depth corrected scaffold vertical coverage was calculated by dividing the relative read abundance by the total scaffold length multiplied by the average number of viral read bases. Read abundance was used where assembly genome fragmentation could impact abundance such as for higher taxonomy level compositional abundance. Vertical coverage was used where genome fragmentation was not expected to be an issue, such as for scaffold abundance, cumulative abundance of scaffolds containing a single gene, or the binned NCV genomes.

Antarctic *Crassvirales* bacteriophages

To identify *Crassvirales* scaffolds, we used a targeted approach that does not depend on protein predictions as *Crassvirales* are known to include alternative genetic codes⁴⁴. First, we used transeq⁹⁸ to obtain the six-frames translations of the DNA scaffolds (options: -frame 6 -table 11 -clean). HMM profiles of the *Crassvirales* phylogenetic marker genes (see ref. 44), including the major capsid protein (MCP), the terminase large subunit (TerL), and the portal protein (portal), were used to search for homologs via hmmscan (HMMER v3.1b2). Hmmscan results were then filtered (e-value < 0.05, coverage > 0.3). Scaffolds over 10 kb in length and containing matches to any of these three proteins were put forward for further inspection as candidate *Crassvirales* ($n = 466$).

To place the candidate *Crassvirales* scaffolds within the larger context of *Caudoviricetes* families, we used the Virus Metadata Resource from the International Committee on Taxonomy of Viruses (VMR_21-221122_MSL37). We selected at random ten isolates (or all if < 10 available) for each of the 43 *Caudoviricetes* families excluding: i) members of the *Crassvirales* order (Feb 2023), and ii) isolates from the *Helgolandviridae* ($n = 1$), *Grauviridae* ($n = 2$), and *Duneeviridae* ($n = 6$) from which no sequences could be extracted using our approach. This resulted in 245 species/isolates for which we obtained genomes,

encoded proteins, and gene annotations from the NCBI Nucleotide database.

To reconstruct the phylogeny, we retrieved the TerL, MCP, and portal proteins encoded in the reference genomes by extracting the proteins containing in their headers “terminase”, excluding “terminase small”, “major head”, “major capsid”, and “portal”, using grep and seqtk subseq (<https://github.com/lh3/seqtk>). We were able to extract the phylogenetic markers from most of the sequences (243 TerL (99.2%), 234 MCP (95.5%) and 185 portal (75.5%) proteins from the 245 genomes), no gene duplicates were detected. In addition, we collected 673 *Crassvirales* genomes and TerL, MCP and portal protein sequences (from refs. 43,44). These sequences were used with those from our candidate *Crassvirales* to build separate phylogenetic trees of each protein. For the multiple sequence alignment, we used MAFFT⁹⁹ (v7.475, option: -auto), modeltest-ng¹⁰⁰ to determine the amino acids substitution model (option: -d aa), and IQ-TREE2 v2.1.1¹⁰¹ to compute the phylogeny (option: -m LG + G4 + F -B 1000). Candidate *Crassvirales* scaffolds for which all three proteins (TerL, MCP, and Portal) that fell within the clade formed by the ICTV-approved *Crassvirales* families were deemed *Crassvirales* sequences.

The ORFs of candidate scaffolds were detected with Prodigal v2.6.3⁹² using three modes to consider stop codon reassignments (options: standard, -TGA W, and -TAG Q). These were functionally annotated using the marker protein HMMs from Yutin et al. 2021 (ref. 44). The trees and their annotation were created using the software suite ggtree v3.6.2¹⁰² and iTOL v5¹⁰³. The genomic maps were built via gggenomes v0.9.5.9¹⁰⁴.

Nucleocytoviricota and Mirusviricota

To identify NCVs, we first binned all assembled scaffolds using vRhyme v1.1.0 for the viral fraction co-assembly and using CONCOCT v1.1.0 for the corresponding cellular fraction assemblies. Scaffolds were examined for *Nucleocytoviricota* markers by performing a hmmsearch on prodigal predicted proteins⁹² (v2.6.3 -p meta) against the nine giant virus orthologous groups HMM profiles using nclv_markersearch⁴⁶. All bins containing hits to phylogenetic marker genes were further investigated. Bins were decontaminated from likely contaminating cellular scaffolds using viralrecall¹⁰⁵ (removing those with score < 0 as per ref. 106). Separate phylogenetic trees for the markers were built by combining the bins with a comprehensive set of NCVs, *Mirusviricota*, *Herpesvirales*, Eukaryotic and Archaeal genomes collected by Karki et al. 2024 (ref. 107), including the recently described NCV class *Mriyaviricetes*⁴⁷. We further removed scaffolds containing markers falling within the Eukaryotic clades for RNA polymerase, DNA topoisomerase I, and DNA polymerase B.

The phylogenetic trees were built for the bins and a reference set containing NCV isolates and metagenomic bins collected from previous metagenomic surveys^{46–48,106,108} and additional RefSeq NCV isolates as of September 2022 (Supplementary data 2). First, by detecting and aligning the seven genetic markers⁴⁶ using nclv_markersearch (VLTF3, A32, TopoII, TFIIB, PolB, RNAPL and SFII). The alignments were trimmed of regions where > 20% of the sequences have a gap and with an entropy score below 0.55 using BMGE v1.12.111. The trimmed alignments were used to build a maximum likelihood tree using IQ-tree2¹⁰¹ the best model finder option (-m MFP) with ultrafast bootstrap of 1000 replicates. Bins were manually assigned a taxonomy based on the reference set taxonomy.

For the final dataset, only bins containing at least four out of seven markers were kept, except for those classified as *Mirusviricota*⁴⁸ and *Mriyaviricetes*⁴⁷ where all bins with at least two markers were kept, since these viral groups not possess all NCV marker genes (see Supplementary data 2 for gene presence/non-detection). The *Mriyaviruses* sequences belonged to large genomic bins which also contained Eukaryotic-like RNA polymerase, DNA topoisomerase II and DNA

polymerase B genes. We removed this Eukaryotic host contamination by retaining only the contigs containing the marker genes VLTF3, A32 and MCP⁴⁷. Bins with more than one duplication of the genes SFII, VLTF3, A32, and PolB were removed to avoid bins with high strain heterogeneity (as per ref. 106). We removed redundant bins by clustering bins at 95% average nucleotide identity or 100% marker gene amino acid identity and selected the best representative (most marker genes or highest N50). Eukaryotic contamination was identified on the NCV bins and the unfiltered *Mriyaviruses* by using MetaEuk v6.a5d39d9¹⁰⁹ to predict (using Pfam reference) and classify (using MMETSP_zenodo_3247846_uniuc190_2018) ORFs.

We used nclv_markersearch to screen the final set of bins for the seven genetic markers⁴⁶, and to perform the alignments and concatenation. The alignment was trimmed of regions where >20% of the sequences had a gap and with an entropy score below 0.55 using BMGE v1.12¹¹⁰. The trimmed alignment was used to build a maximum likelihood tree using iqtree2¹⁰¹ the best model finder option (-m MFP) with ultrafast bootstrap of 1000 replicates. The best fit model was LG + F + R10. The tree was visualized using FigTree v1.4.4¹¹¹.

Maveriviricetes and Polintonviricetes viruses

All scaffolds were inspected for virophages (class *Maveriviricetes*) and polinton-like viruses (PLVs, class *Polintonviricetes*) major capsid protein (MCP) using a collection HMM built using global, and clade restricted protein alignments. Rothera scaffolds ORFs were predicted and translated to amino acid using prodigal⁹² (v2.6.3 -p meta).

For the *Maveriviricetes*, we used a collection of non-redundant isolate and metagenomic MCP sequences⁵². The global and family rank MCP alignments were built with MAFFT⁹⁹ (v7.407, -auto), and the HMM profile built with hmmbuild¹¹² 2 (HMMER v3.1b2). We used these profiles to identify putative virophage MCPs in the Rothera scaffolds' amino acid sequences (> 200 aa) using hmmsearch (HMMER v3.1b2). The new putative virophage MCP were joined with the reference sequences and the *Maveriviricetes* phylogeny was built, and the sequences classified according to the newly proposed taxonomy (ref. 52).

For PLVs, HMM profiles were constructed using the MCP genes from a collection of curated PLV sequences^{34,57}. PLV MCP identified in Yutin et al., 2015 (ref. 34) were used as queries to search the non-redundant NCBI protein database. The hits were collected, clustered with UCLUST¹¹³ with a similarity threshold of 0.5 and were iteratively aligned and clustered using the approach described by Wolf et al., 2018 (ref. 114). From the alignment of the cluster containing the query proteins, a tree was built using FastTree¹¹⁵. From the tree topology eight clades were manually inferred for which separate HMM profiles were built. Translated Rothera scaffolds were searched with these HMM profiles and the profiles provided by Bellas and Sommaruga, 2021 (ref. 57). The hits were mixed with reference PLV MCPs (proteins of the HMM profiles). The resulting protein set was iteratively aligned and clustered using the abovementioned approach, and the alignment of the protein cluster containing reference PLV MCPs was used to build a tree using FastTree. Tree clades were named according to the clades as defined in Yutin et al., 2015 and Bellas and Sommaruga, 2021 (refs. 34,57).

For the functional annotation of the other virophage genes, all predicted proteins from putative virophage scaffolds were pooled with proteins predicted from virophage genomes available from Roux et al. 2023 (ref. 52). Proteins were clustered using mmseqs easy-cluster¹¹⁶, and for each cluster, alignments and profiles were generated by MAFFT⁹⁹ (v7.505, -einsi), hhconsensus¹¹⁷ (v3.3.0) and finally hhmake¹¹⁷ (v3.3.0). All profiles were then searched against the Pfam (<http://pfam.xfam.org/>) and PDB (<https://www.rcsb.org/>) databases using hhsearch¹¹⁷ (v3.3.0, -E 1e-4). Matches with at least 90% probability, e-values below 1e-4, clear functional annotation as well as a

score that was at least 90% of the best score per cluster were used for annotation. Annotation of PLV scaffolds was performed similarly to the virophages, with all predicted proteins from putative PLV scaffolds being pooled with proteins predicted from available PLV genomes^{34,57}. We additionally searched the profiles against a database consisting of the profiles of clusters from Bellas and Sommaruga 2021 (ref. 57) and transferred annotations. The annotated genomes were visualized using gggenomes¹⁰⁴ in combination with ggtree¹⁰².

For all NCV bins, predicted proteins were searched against the GVDB database using HMMER v3.3.2. Upstream regions (50 bp) of genes homologous to *Cafeteria roenbergensis* virus 'late' genes were extracted from the genomes and searched for enriched motifs using the streme tool from the meme-suite v5.5.0 and the protein-coding regions as negative controls. Candidate motifs were filtered for non-AT consensus sites and scores below $1e^{-3}$. Similarly, upstream regions of all virophage genes were extracted and searched for enriched occurrences of these candidate motifs using the sea tool (--thresh 1) from the meme-suite, again using the protein-coding regions as negative controls. PLV scaffolds above 5,000 bps were analyzed similarly for occurrences of a consensus 'early' NCV promoter motif (WWWWWGTGWWWW).

Viral diversity and correlation with environmental parameters

We performed a multivariate analysis on viral sequences of high and mid quality (longer than 10 kb or at least 70% complete) to avoid highly fragmented genomes. Given the compositional nature of the abundance data, the analysis was performed using compositional data analysis methods¹¹⁸. Viral read abundance was normalized by sequence length and centered-log ratio transformation using microbiome R package v1.20.0 (<https://github.com/microbiome/microbiome>). We explored the seasonal dynamics of alpha diversity by calculating the species richness and the Shannon and inverse Simpson diversity indexes for each day using hillR v0.5.1¹¹⁹, which are expressed in effective number of species. Simpson evenness was calculated by dividing the inverse Simpson index by the species richness. Additionally, we tracked the number and abundance of dominant viruses, defined as viral scaffolds representing over 0.5% of the viral reads at any given time ($n = 203$).

We performed a hierarchical cluster analysis based of the Aitchison distance using hclust¹²⁰ (method centroid), and the normalized abundances visualized in heatmap using the stats package in R.

Microbial abundances and Chl-a concentrations were log-transformed and other environmental metadata was visually checked for normality and z-scored or log transformed to achieve a distribution closest to normal. Pairwise Pearson correlation was computed and from strongly covarying environmental metadata pairs, one was removed ($r > 0.8$). To find which combination of variables better correlated with changes in the viral community, we fitted a general multivariate regression model to our data using Adonis2 (vegan v2.6-4)¹²¹. Variables were sequentially permuted so that the variables were input to the model by order of highest sum of squares, non-significant variables were removed from the model. The association between the phage and bacterial communities were tested by using a partial Mantel test on the Aitchison distance matrixes, while controlling for environmental conditions using the mantel.partial function (Pearson correlation and 999 permutations, Vegan v2.6-4). The control environmental matrix was computed as the Euclidean distances of the non-covarying variables which were significant according to the general multivariate regression model.

Reporting summary

Further information on research design is available in the Nature Portfolio Reporting Summary linked to this article.

Data availability

Metagenomic raw reads have been deposited in the European Nucleotide Archive under the Bioproject PRJEB71789. Figure source data are provided with this paper. The sampling metadata, used HHM profiles, viral scaffold nucleotide sequences, NCV bins, taxonomic and host annotations, viral marker gene protein alignments and phylogenies are available through the NIOZ dataverse <https://doi.org/10.25850/nioz/7b.b.wg>. Source data are provided with this paper.

References

- Suttle, C. A. Marine viruses - Major players in the global ecosystem. *Nat. Rev. Microbiol.* **5**, 801–812 (2007).
- Fuhrman, J. A. Marine viruses and their biogeochemical and ecological effects. *Nature* **399**, 541–548 (1999).
- López-García, P. et al. Metagenome-derived virus-microbe ratios across ecosystems. *ISME J.* **17**, 1552–1563 (2023).
- Bar-On, Y. M. & Milo, R. The Biomass Composition of the Oceans: A Blueprint of Our Blue Planet. *Cell* **179**, 1451–1454 (2019).
- Brum, J. R. & Sullivan, M. B. Rising to the challenge: accelerated pace of discovery transforms marine virology. *Nat. Rev. Microbiol.* **13**, 147–159 (2015).
- Sullivan, M. B., Weitz, J. S. & Wilhelm, S. Viral ecology comes of age. *Environ. Microbiol. Rep.* **9**, 33–35 (2017).
- Breitbart, M. et al. Genomic analysis of uncultured marine viral communities. *Proc. Natl. Acad. Sci.* **99**, 14250–14255 (2002).
- Gregory, A. C. et al. Marine DNA viral macro- and microdiversity from Pole to Pole. *Cell* **177**, 1109–1123 (2019).
- Roux, S. et al. Ecogenomics and potential biogeochemical impacts of globally abundant ocean viruses. *Nature* **537**, 689–693 (2016).
- Luo, E., Leu, A. O., Eppley, J. M., Karl, D. M. & DeLong, E. F. Diversity and origins of bacterial and archaeal viruses on sinking particles reaching the abyssal ocean. *ISME J.* **16**, 1627–1635 (2022).
- Ignacio-Espinoza, J. C., Ahlgren, N. A. & Fuhrman, J. A. Long-term stability and Red Queen-like strain dynamics in marine viruses. *Nat. Microbiol.* **5**, 265–271 (2019).
- Coutinho, F. H. et al. Marine viruses discovered via metagenomics shed light on viral strategies throughout the oceans. *Nat. Commun.* **8**, 1–12 (2017).
- Cassman, N. et al. Oxygen minimum zones harbour novel viral communities with low diversity. *Environ. Microbiol.* **14**, 3043–3065 (2012).
- Heinrichs, M. E. et al. Breaking the Ice: A Review of Phages in Polar Ecosystems. in 31–71. https://doi.org/10.1007/978-1-0716-3549-0_3 (Humana, New York, NY, 2024).
- Marshall, J. & Speer, K. Closure of the meridional overturning circulation through Southern Ocean upwelling. *Nat. Geosci.* **5**, 171–180 (2012).
- Frölicher, T. L. et al. Dominance of the Southern Ocean in Anthropogenic Carbon and Heat Uptake in CMIP5 Models. *J. Clim.* **28**, 862–886 (2015).
- Huang, Y., Fassbender, A. J. & Bushinsky, S. M. Biogenic carbon pool production maintains the Southern Ocean carbon sink. *Proc. Natl. Acad. Sci. USA.* **120**, e2217909120 (2023).
- Biggs, T. E. G. et al. Antarctic phytoplankton community composition and size structure: importance of ice type and temperature as regulatory factors. *Polar Biol.* **42**, 1997–2015 (2019).
- Venables, H. J., Clarke, A. & Meredith, M. P. Wintertime controls on summer stratification and productivity at the western Antarctic Peninsula. *Limnol. Oceanogr.* **58**, 1035–1047 (2013).
- Luria, C. M. et al. Seasonal shifts in bacterial community responses to phytoplankton-derived dissolved organic matter in the Western Antarctic Peninsula. *Front. Microbiol.* **8**, 2117 (2017).

21. Carvalho, F., Kohut, J., Oliver, M. J., Sherrell, R. M. & Schofield, O. Mixing and phytoplankton dynamics in a submarine canyon in the West Antarctic Peninsula. *J. Geophys. Res. Ocean.* **121**, 5069–5083 (2016).
22. Evans, C. & Brussaard, C. P. D. Regional variation in lytic and lysogenic viral infection in the southern ocean and its contribution to biogeochemical cycling. *Appl. Environ. Microbiol.* **78**, 6741–6748 (2012).
23. Brum, J. R., Hurwitz, B. L., Schofield, O., Ducklow, H. W. & Sullivan, M. B. Seasonal time bombs: Dominant temperate viruses affect Southern Ocean microbial dynamics. *ISME J.* **10**, 437–449 (2016).
24. Biggs, T. E. G., Huisman, J. & Brussaard, C. P. D. Viral lysis modifies seasonal phytoplankton dynamics and carbon flow in the Southern Ocean. *ISME J.* **15**, 3615–3622 (2021).
25. Evans, C. et al. Shift from Carbon Flow through the Microbial Loop to the Viral Shunt in Coastal Antarctic Waters during Austral Summer. *Microorganisms* **9**, 460 (2021).
26. Eich, C. et al. Ecological Importance of Viral Lysis as a Loss Factor of Phytoplankton in the Amundsen Sea. *Microorganisms* **10**, 1967 (2022).
27. Yang, Q. et al. Metagenomic Characterization of the Viral Community of the South Scotia Ridge. *Viruses* **11**, 95 (2019).
28. Gong, Z. et al. Viral Diversity and Its Relationship With Environmental Factors at the Surface and Deep Sea of Prydz Bay, Antarctica. *Front. Microbiol.* **9**, 2981 (2018).
29. Alarcón-Schumacher, T., Guajardo-Leiva, S., Martínez-García, M. & Díez, B. Ecogenomics and Adaptation Strategies of Southern Ocean Viral Communities. *mSystems* **6**, e0039621 (2021).
30. Lopez-Simon, J. et al. Viruses under the Antarctic Ice Shelf are active and potentially involved in global nutrient cycles. *Nat. Commun.* **14**, 1–10 (2023).
31. Nayfach, S. et al. CheckV assesses the quality and completeness of metagenome-assembled viral genomes. *Nat. Biotechnol.* **39**, 578–585 (2020).
32. Jiang, J.-Z. et al. Virus classification for viral genomic fragments using PhaGCN2. *Brief. Bioinform.* **24**, bbac505 (2023).
33. Bellas, C. et al. Large-scale invasion of unicellular eukaryotic genomes by integrating DNA viruses. *Proc. Natl Acad. Sci. USA.* **120**, e2300465120 (2023).
34. Yutin, N., Shevchenko, S., Kapitonov, V., Krupovic, M. & Koonin, E. V. A novel group of diverse Polinton-like viruses discovered by metagenome analysis. *BMC Biol.* **13**, 1–14 (2015).
35. Roux, S. et al. Towards quantitative viromics for both double-stranded and single-stranded DNA viruses. *PeerJ* **2016**, e2777 (2016).
36. Breitbart, M., Delwart, E., Rosario, K., Segalés, J. & Varsani, A. ICTV virus taxonomy profile: Circoviridae. *J. Gen. Virol.* **98**, 1997–1998 (2017).
37. Venables, H. et al. Sustained year-round oceanographic measurements from Rothera Research Station, Antarctica, 1997–2017. *Sci. Data* **10**, 1–13 (2023).
38. Roux, S. et al. iPhoP: An integrated machine learning framework to maximize host prediction for metagenome-derived viruses of archaea and bacteria. *PLoS Biol.* **21**, e3002083 (2023).
39. Straza, T. R. A., Ducklow, H. W., Murray, A. E. & Kirchman, D. L. Abundance and single-cell activity of bacterial groups in Antarctic coastal waters. *Limnol. Oceanogr.* **55**, 2526–2536 (2010).
40. Sow, S. L. S. et al. Biogeography of Southern Ocean prokaryotes: a comparison of the Indian and Pacific sectors. *Environ. Microbiol.* **24**, 2449–2466 (2022).
41. Luria, C. M., Amaral-Zettler, L. A., Ducklow, H. W. & Rich, J. J. Seasonal succession of free-living bacterial communities in coastal waters of the western antarctic peninsula. *Front. Microbiol.* **7**, 1731 (2016).
42. Turner, D. et al. Abolishment of morphology-based taxa and change to binomial species names: 2022 taxonomy update of the ICTV bacterial viruses subcommittee. *Arch. Virol.* **168**, 74 (2023).
43. Yutin, N. et al. Discovery of an expansive bacteriophage family that includes the most abundant viruses from the human gut. *Nat. Microbiol.* **3**, 38–46 (2018).
44. Yutin, N. et al. Analysis of metagenome-assembled viral genomes from the human gut reveals diverse putative CrAss-like phages with unique genomic features. *Nat. Commun.* **12**, 1–11 (2021).
45. Abergel, C., Legendre, M. & Claverie, J. M. The rapidly expanding universe of giant viruses: Mimivirus, Pandoravirus, Pithovirus and Mollivirus. *FEMS Microbiol. Rev.* **39**, 779–796 (2015).
46. Aylward, F. O., Moniruzzaman, M., Ha, A. D. & Koonin, E. V. A phylogenomic framework for charting the diversity and evolution of giant viruses. *PLoS Biol.* **19**, e3001430 (2021).
47. Yutin, N., Mutz, P., Krupovic, M. & Koonin, E. V. Mriyaviruses: small relatives of giant viruses. *MBio* <https://doi.org/10.1128/mbio.01035-24> (2024).
48. Gaïa, M. et al. Mirusviruses link herpesviruses to giant viruses. *Nature* **616**, 783–789 (2023).
49. Gallot-Lavallée, L. et al. The 474-Kilobase-Pair Complete Genome Sequence of CeV-01B, a Virus Infecting Haptolina (*Chrysochromulina*) ericina (Prymnesiophyceae). *Genome Announc* **3**, e01413–e01415 (2015).
50. Santini, S. et al. Genome of *Phaeocystis globosa* virus PgV-16T highlights the common ancestry of the largest known DNA viruses infecting eukaryotes. *Proc. Natl Acad. Sci. USA.* **110**, 10800–10805 (2013).
51. Roitman, S. et al. Isolation and infection cycle of a polinton-like virus virophage in an abundant marine alga. *Nat. Microbiol.* **8**, 332–346 (2023).
52. Roux, S. et al. Updated Virophage Taxonomy and Distinction from Polinton-like Viruses. *Biomolecules* **13**, 204 (2023).
53. Yutin, N., Raoult, D. & Koonin, E. V. Virophages, polintons, and transpovirons: A complex evolutionary network of diverse selfish genetic elements with different reproduction strategies. *Virol. J.* **10**, 1–15 (2013).
54. Yau, S. et al. Virophage control of antarctic algal host-virus dynamics. *Proc. Natl Acad. Sci. USA.* **108**, 6163–6168 (2011).
55. Fischer, M. G. & Suttle, C. A. A virophage at the origin of large DNA transposons. *Science.* **332**, 231–234 (2011).
56. Roux, S. et al. Ecogenomics of virophages and their giant virus hosts assessed through time series metagenomics. *Nat. Commun.* **8**, 1–12 (2017).
57. Bellas, C. M. & Sommaruga, R. Polinton-like viruses are abundant in aquatic ecosystems. *Microbiome* **9**, 1–14 (2021).
58. Dutilh, B. E. et al. A highly abundant bacteriophage discovered in the unknown sequences of human faecal metagenomes. *Nat. Commun.* **5**, 1–11 (2014).
59. Edwards, R. A. et al. Global phylogeography and ancient evolution of the widespread human gut virus crAssphage. *Nat. Microbiol.* **4**, 1727–1736 (2019).
60. Fischer, M. G. & Hackl, T. Host genome integration and giant virus-induced reactivation of the virophage mavirus. *Nature* **540**, 288–291 (2016).
61. Koonin, E. V. & Krupovic, M. Polintons, virophages and transpovirons: a tangled web linking viruses, transposons and immunity. *Curr. Opin. Virol.* **25**, 7–15 (2017).
62. Pagarete, A., Grébert, T., Stepanova, O., Sandaa, R. A. & Bratbak, G. Tsv-N1: A Novel DNA Algal Virus that Infects *Tetraselmis striata*. *Viruses* **7**, 3937 (2015).
63. Brussaard, C. P. D. Viral Control of Phytoplankton Populations—a Review1. *J. Eukaryot. Microbiol.* **51**, 125–138 (2004).

64. Moreau, H. et al. Marine Prasinovirus Genomes Show Low Evolutionary Divergence and Acquisition of Protein Metabolism Genes by Horizontal Gene Transfer. *J. Virol.* **84**, 12555–12563 (2010).
65. Yau, S. et al. Virus-host coexistence in phytoplankton through the genomic lens. *Sci. Adv.* **6**, eaay2587 (2020).
66. Alarcón-Schumacher, T., Guajardo-Leiva, S., Antón, J. & Díez, B. Elucidating viral communities during a phytoplankton bloom on the west Antarctic Peninsula. *Front. Microbiol.* **10**, 1014 (2019).
67. Sheik, A. R. et al. Responses of the coastal bacterial community to viral infection of the algae *Phaeocystis globosa*. *ISME J.* **8**, 212–225 (2013).
68. Massom, R. A. et al. Antarctic ice shelf disintegration triggered by sea ice loss and ocean swell. *Nature* **558**, 383–389 (2018).
69. Williams, T. J. et al. The role of planktonic Flavobacteria in processing algal organic matter in coastal East Antarctica revealed using metagenomics and metaproteomics. *Environ. Microbiol.* **15**, 1302–1317 (2013).
70. Piontek, J., Meeske, C., Hassenrück, C., Engel, A. & Jürgens, K. Organic matter availability drives the spatial variation in the community composition and activity of Antarctic marine bacterioplankton. *Environ. Microbiol.* **24**, 4030–4048 (2022).
71. Tada, Y., Makabe, R., Kasamatsu-Takazawa, N., Taniguchi, A. & Hamasaki, K. Growth and distribution patterns of *Roseobacter/Rhodobacter*, SAR11, and *Bacteroidetes* lineages in the Southern Ocean. *Polar Biol.* **36**, 691–704 (2013).
72. Silveira, C. B., Luque, A. & Rohwer, F. The landscape of lysogeny across microbial community density, diversity and energetics. *Environ. Microbiol.* **23**, 4098–4111 (2021).
73. Clarke, A., Meredith, M. P., Wallace, M. I., Brandon, M. A. & Thomas, D. N. Seasonal and interannual variability in temperature, chlorophyll and macronutrients in northern Marguerite Bay, Antarctica. *Deep Sea Res. Part II Top. Stud. Oceanogr.* **55**, 1988–2006 (2008).
74. Hurwitz, B. L., Deng, L., Poulos, B. T. & Sullivan, M. B. Evaluation of methods to concentrate and purify ocean virus communities through comparative, replicated metagenomics. *Environ. Microbiol.* **15**, 1428–1440 (2013).
75. Brussaard, C. P. D., Payet, J. P., Winter, C. & Weinbauer, M. G. Quantification of aquatic viruses by flow cytometry. in *Manual of Aquatic Viral Ecology* 102–109 <https://doi.org/10.4319/mave.2010.978-0-9845591-0-7.102> (American Society of Limnology and Oceanography, 2010).
76. Mojica, K. D. A., Evans, C. & Brussaard, C. P. D. Flow cytometric enumeration of marine viral populations at low abundances. *Aquat. Microb. Ecol.* **71**, 203–209 (2014).
77. Marie, D., Partensky, F., Vaulot, D. & Brussaard, C. Enumeration of Phytoplankton, Bacteria, and Viruses in Marine Samples. *Curr. Protoc. Cytom.* **10**, 11.11.1–11.11.15 (1999).
78. van Leeuwe, M. A., Villerius, L. A., Roggeveld, J., Visser, R. J. W. & Stefels, J. An optimized method for automated analysis of algal pigments by HPLC. *Mar. Chem.* **102**, 267–275 (2006).
79. Van Heukelem, L. & Thomas, C. S. Computer-assisted high-performance liquid chromatography method development with applications to the isolation and analysis of phytoplankton pigments. *J. Chromatogr. A* **910**, 31–49 (2001).
80. Strickland, J. D. H. & Parsons, T. R. *A Practical Handbook of Seawater Analysis*. Ottawa: Fisheries Research Board of Canada, Bulletin 167. *Internationale Revue der gesamten Hydrobiologie und Hydrographie* vol. **55** (1972).
81. Murphy, J. & Riley, J. P. A modified single solution method for the determination of phosphate in natural waters. *Anal. Chim. Acta* **27**, 31–36 (1962).
82. Grasshoff, K., Kremling, K. & Ehrhardt, M. *Methods of seawater analysis*. (1983).
83. Ewels, P., Magnusson, M., Lundin, S. & Käller, M. MultiQC: summarize analysis results for multiple tools and samples in a single report. *Bioinformatics* **32**, 3047–3048 (2016).
84. Schmieder, R. & Edwards, R. Quality control and preprocessing of metagenomic datasets. *Bioinformatics* **27**, 863–864 (2011).
85. Bolger, A. M., Lohse, M. & Usadel, B. Trimmomatic: a flexible trimmer for Illumina sequence data. *Bioinformatics* **30**, 2114–2120 (2014).
86. Zolfo, M. et al. Detecting contamination in viromes using Vir-omeQC. *Nat. Biotechnol.* **2019** 3712 **37**, 1408–1412 (2019).
87. Gruber-Vodicka, H. R., Seah, B. K. B. & Pruesse, E. phyloFlash: Rapid Small-Subunit rRNA Profiling and Targeted Assembly from Metagenomes. *mSystems* **5**, e00920 (2020).
88. Nurk, S., Meleshko, D., Korobeynikov, A. & Pevzner, P. A. metaSPAdes: a new versatile metagenomic assembler. *Genome Res* **27**, 824–834 (2017).
89. Fang, Z. et al. PPR-Meta: a tool for identifying phages and plasmids from metagenomic fragments using deep learning. *Gigascience* **8**, 1–14 (2019).
90. Wu, L.-Y. et al. Benchmarking bioinformatic virus identification tools using real-world metagenomic data across biomes. *Genome Biol* **25**, 97. <https://doi.org/10.1186/s13059-024-03236-4> (2024).
91. Tisza, M. J., Belford, A. K., Dominguez-Huerta, G., Bolduc, B. & Buck, C. B. Cenote-Taker 2 democratizes virus discovery and sequence annotation. *Virus Evol.* **7**, veaa100 (2021).
92. Hyatt, D. et al. Prodigal: Prokaryotic gene recognition and translation initiation site identification. *BMC Bioinforma.* **11**, 1–11 (2010).
93. Bin Jang, H. et al. Taxonomic assignment of uncultivated prokaryotic virus genomes is enabled by gene-sharing networks. *Nat. Biotechnol.* **37**, 632–639 (2019).
94. Shannon, P. et al. Cytoscape: a software environment for integrated models of biomolecular interaction networks. *Genome Res.* **13**, 2498–2504 (2003).
95. Li, H. Aligning sequence reads, clone sequences and assembly contigs with BWA-MEM. <https://doi.org/10.48550/arxiv.1303.3997> (2013).
96. Robbins, S. J. et al. A genomic view of the reef-building coral *Porites lutea* and its microbial symbionts. *Nat. Microbiol.* **4**, 2090–2100 (2019).
97. Li, H. et al. The Sequence Alignment/Map format and SAMtools. *Bioinformatics* **25**, 2078–2079 (2009).
98. Rice, P., Longden, L. & Bleasby, A. EMBOSS: The European Molecular Biology Open Software Suite. *Trends Genet* **16**, 276–277 (2000).
99. Katoh, K. & Standley, D. M. MAFFT multiple sequence alignment software version 7: Improvements in performance and usability. *Mol. Biol. Evol.* **30**, 772–780 (2013).
100. Darriba, D. et al. ModelTest-NG: A New and Scalable Tool for the Selection of DNA and Protein Evolutionary Models. *Mol. Biol. Evol.* **37**, 291–294 (2020).
101. Minh, B. Q. et al. IQ-TREE 2: New Models and Efficient Methods for Phylogenetic Inference in the Genomic Era. *Mol. Biol. Evol.* **37**, 1530–1534 (2020).
102. Yu, G., Smith, D. K., Zhu, H., Guan, Y. & Lam, T. T. Y. ggtree: an R package for visualization and annotation of phylogenetic trees with their covariates and other associated data. *Methods Ecol. Evol.* **8**, 28–36 (2017).
103. Letunic, I. & Bork, P. Interactive Tree Of Life (iTOL) v5: an online tool for phylogenetic tree display and annotation. *Nucleic Acids Res.* **49**, W293–W296 (2021).
104. Hackl, T., Duponchel, S., Barenhoff, K., Weinmann, A. & Fischer, M. G. Virophages and retrotransposons colonize the genomes of a heterotrophic flagellate. *Elife* **10**, e72674 (2021).

105. Aylward, F. O. & Moniruzzaman, M. ViralRecall—A Flexible Command-Line Tool for the Detection of Giant Virus Signatures in ‘Omic Data. *Viruses* **13**, 150 (2021).
106. Moniruzzaman, M., Martinez-Gutierrez, C. A., Weinheimer, A. R. & Aylward, F. O. Dynamic genome evolution and complex virocell metabolism of globally-distributed giant viruses. *Nat. Commun.* **11**, 1–11 (2020).
107. Karki, S., Barth, Z. K., Aylward, F. O. Chimeric origin of eukaryotes from Asgard archaea and ancestral giant viruses. *bioRxiv* 4–6 <https://doi.org/10.1101/2024.04.22.590592> (2024).
108. Schulz, F. et al. Giant virus diversity and host interactions through global metagenomics. *Nature* **578**, 432–436 (2020).
109. Levy Karin, E., Mirdita, M. & Söding, J. MetaEuk-sensitive, high-throughput gene discovery, and annotation for large-scale eukaryotic metagenomics. *Microbiome* **8**, 1–15 (2020).
110. Criscuolo, A. & Gribaldo, S. BMGE (Block Mapping and Gathering with Entropy): A new software for selection of phylogenetic informative regions from multiple sequence alignments. *BMC Evol. Biol.* **10**, 1–21 (2010).
111. Rambaut, A. FigTree v1.4.4 (2018).
112. Eddy, S. R. Accelerated profile HMM searches. *PLoS Comput. Biol.* **7**, e1002195 (2011).
113. Edgar, R. C. Search and clustering orders of magnitude faster than BLAST. *Bioinformatics* **26**, 2460–2461 (2010).
114. Wolf, Y. I. et al. Origins and Evolution of the Global RNA Virome. *MBio* **9**, e02329–18 (2018).
115. Price, M. N., Dehal, P. S. & Arkin, A. P. FastTree 2 – Approximately Maximum-Likelihood Trees for Large Alignments. *PLoS One* **5**, e9490 (2010).
116. Steinegger, M. & Söding, J. MMseqs2 enables sensitive protein sequence searching for the analysis of massive data sets. *Nat. Biotechnol.* **35**, 1026–1028 (2017).
117. Steinegger, M. et al. HH-suite3 for fast remote homology detection and deep protein annotation. *BMC Bioinforma.* **20**, 1–15 (2019).
118. Gloor, G. B., Macklaim, J. M., Pawlowsky-Glahn, V. & Egozcue, J. J. Microbiome datasets are compositional: And this is not optional. *Front. Microbiol.* **8**, 294209 (2017).
119. Li, D. hillR: taxonomic, functional, and phylogenetic diversity and similarity through Hill Numbers. *J. Open Source Softw.* **3**, 1041 (2018).
120. Murtagh, F. & Legendre, P. Ward’s Hierarchical Agglomerative Clustering Method: Which Algorithms Implement Ward’s Criterion? *J. Classif.* **31**, 274–295 (2014).
121. McArdle, B. H. & Anderson, M. J. Fitting multivariate models to community data: A comment on distance-based redundancy analysis. *Ecology* **82**, 290–297 (2001).
- 2051 – Project-ID 39071386 (B.E.D), the European Union’s Horizon 2020 research and innovation program, under the Marie Skłodowska-Curie Actions Innovative Training Networks grant agreement no. 955974 (VIROINF, B.E.D), the Alexander von Humboldt Foundation in the context of an Alexander von Humboldt-Professorship founded by the German Federal Ministry of Education and Research (B.E.D), and a junior researcher fellowship from the Fonds voor Wetenschappelijk Onderzoek (FWO) [12D8623N, C.L.].

Author contributions

G.J.P., C.P.D.B., and B.E.D. designed the study. E.M.W. and G.J.P. collected all samples. G.J.P. processed and analyzed the data. T.E.G.B. analyzed the environmental metadata. G.J.P., M.E.S, N.Y., and M.G.F. designed and performed the viroplage and polinton-like virus analysis. C.L. and M.V.F. designed and performed the crassphage analysis. G.J.P. and L.W. designed and performed the phage host prediction analysis. G.J.P. took the lead in writing. C.P.D.B. conceived the study and helped shape the research, overall direction and writing of the manuscript. B.E.D. helped shape the analyses and provide critical feedback. H.B. and L.W. helped revise the manuscript. All authors provided feedback on the results and manuscript.

Competing interests

The authors declare no competing interests.

Additional information

Supplementary information The online version contains supplementary material available at <https://doi.org/10.1038/s41467-024-53317-y>.

Correspondence and requests for materials should be addressed to Gonçalo J. Piedade or Corina P. D. Brussaard.

Peer review information *Nature Communications* thanks the anonymous reviewers for their contribution to the peer review of this work. A peer review file is available.

Reprints and permissions information is available at <http://www.nature.com/reprints>

Publisher’s note Springer Nature remains neutral with regard to jurisdictional claims in published maps and institutional affiliations.

Open Access This article is licensed under a Creative Commons Attribution-NonCommercial-NoDerivatives 4.0 International License, which permits any non-commercial use, sharing, distribution and reproduction in any medium or format, as long as you give appropriate credit to the original author(s) and the source, provide a link to the Creative Commons licence, and indicate if you modified the licensed material. You do not have permission under this licence to share adapted material derived from this article or parts of it. The images or other third party material in this article are included in the article’s Creative Commons licence, unless indicated otherwise in a credit line to the material. If material is not included in the article’s Creative Commons licence and your intended use is not permitted by statutory regulation or exceeds the permitted use, you will need to obtain permission directly from the copyright holder. To view a copy of this licence, visit <http://creativecommons.org/licenses/by-nc-nd/4.0/>.

© The Author(s) 2024

Acknowledgements

This work was funded by the POMVIDDY project (grant ALWPP.2016.019 awarded to C.P.D.B.) which was supported by the Dutch Research Council (NWO), within the Netherlands Polar Programme. We are grateful to the British Antarctic Survey, Cambridge, UK, and the MMB-NIOZ technical staff for the logistical and technical support, as well as Nisma Abdelmalik and Monika Krolikowski for field assistance and Gosse Metz for the Sterivex DNA extractions. We thank the NIOZ Nutrient Lab on Texel for performing the inorganic nutrient analysis. We are grateful to Alejandro Abdala, Julia Engelmann and Nina Dombrowsky for providing the functional annotation pipeline. This work was supported by the European Research Council (ERC) Consolidator grant 865694: DiversiPHI (B.E.D), the Deutsche Forschungsgemeinschaft (DFG, German Research Foundation) under Germany’s Excellence Strategy – EXC